

Contents lists available at ScienceDirect

Transportation Research Part B

journal homepage: www.elsevier.com/locate/trb





cooperative trajectory control for synchronizing the movement of two connected and autonomous vehicles separated in a mixed traffic flow

Jiahua Qiu, Lili Du

Department of Civil and Coastal Engineering, University of Florida, Gainesville, FL 32608, USA

ARTICLE INFO

Keywords: Connected and autonomous vehicles Vehicle synchronization Model predictive control Mixed-integer nonlinear programming

ABSTRACT

When connected and autonomous vehicles (CAVs) are widely used in the future, we can foresee many essential applications, such as platoon formation and autonomous police patrolling, which need two CAVs, initially separated in a mixed traffic flow involving CAVs and human-drive vehicles (HDVs), to quickly approach each other and then keep a stable car-following mode. The entire process should not jeopardize surrounding traffic safety and efficiency. The existing literature has not studied this CAV synchronization control well, and this study seeks to make up this gap partially. To do that, we developed a Model Predictive Control model embedded with a mixed-integer nonlinear program (MINLP-MPC), which integrates micro- and macro-traffic flow models to capture hybrid traffic flow dynamics. Specifically, the MPC will generate control law at each discrete timestamp to manage the microscopic movements of the two subject CAVs while predicting their neighboring vehicles' movement by well-accepted car-following models and estimating the distant upstream traffic' response by the macroscopic traffic model such as cell transmission model (CTM). The MINLP-MPC is multi-objective, seeking to sustain both synchronization and traffic efficiencies. To generate such well-balanced optimal control, we noticed that the synchronization experiences two distinct phases, sequentially completing the catch-up and platooning tasks. Accordingly, we transferred MINLP-MPC to a hybrid MPC system consisting of two sequential MPCs, respectively prioritizing the catch-up and platooning control. Then, we developed a weighting strategy to tune the control priorities adaptively. The recursive feasibility of the MPC is mathematically proved. Furthermore, we generalized the MPC and the hybrid MPC system to enable multi-vehicle synchronization. A numerical study built upon the NGSIM dataset demonstrates the efficiency and effectiveness of our approaches under different congestion levels and CAV penetrations.

1. Introduction

Connected and Autonomous Vehicles (CAVs), equipped with wireless communication and automation capabilities, bring great opportunities to develop cooperative driving (Milanés and Shladover, 2014; Vahidi and Sciarretta, 2018) in the future. Existing literature has investigated this potential for different traffic scenarios, such as vehicle platooning (Čičić and Johansson, 2019; Dey et al., 2015; Liang et al., 2015; Vahidi and Sciarretta, 2018; Wang et al., 2018; Zhang et al., 2022) on a highway segment, cooperative

E-mail address: lilidu@ufl.edu (L. Du).

^{*} Corresponding author.

lane change and merging at mainline and on-ramp (or off-ramp) highway intersection (Bevly et al., 2016; Mu et al., 2021; Rios-Torres and Malikopoulos, 2016), and cooperative urban intersection control for CAV fleet (Ashtiani et al., 2018; Yang et al., 2016; Zohdy and Rakha, 2012). This study shares the same research interests in developing cooperative driving, but particularly focuses on the scenario in which two designated CAVs want to approach each other quickly and then keep a stable car-following mode, while thy are originally initially separated by other vehicles (e.g., CAVs or human-drive vehicles (HDVs)) in same or different lanes. We name this type of cooperative driving CAV synchronization control (shortened as synchronization control hereafter).

In the era of CAVs in the future, we can foresee many important applications of this synchronization control. The following only exemplifies a few. First, scholars and OEMs have been aware that CAVs from different manufacturers, such as Tesla and Nissan, will most likely install different cruise control algorithms and they are potentially incompatible (Bhoopalam et al., 2018). Then, when a single CAV drives on the road, it may want to approach the other CAV nearby from the same manufacturer to form a short platoon and benefit from cruise control. In addition, it was recognized that CAVs' frequent lane changes disrupt the flow (Woo and Skabardonis, 2021). As a result, it may not be proper to have multiple CAVs simultaneously for a long platoon, especially when it comes to heavy-duty trucks. Accordingly, an existing study considers a platoon formation scheme to have one heavy-duty CAV truck approach another first to form a short platoon and gradually increase the platoon size (Liang et al., 2015). Besides, there are more futuristic applications when CAVs are combined with other emerging technologies. For example, existing studies (Hallmark et al., 2019; Subedi et al., 2020) showed that CAVs could potentially be used for police patrolling activity, where a CAV patrol detects and sends warnings to a speeding CAV and then catches up without triggering a siren to disrupt the traffic. Moreover, by combining CAV and advanced battery-to-battery charging technologies, both scholars and practitioners (Abdolmaleki et al., 2019; Chakraborty et al., 2020; Kosmanos et al., 2018; Maglaras et al., 2014) have investigated emerging mobile vehicle-to-vehicle charging services, which dispatch one electric vehicle (CAV) to approach and then charge another electric vehicle (EV) on-the-move. This new mobile charging service calls for efficient synchronization control so that we can have one EV on a road catch up with the other EV and then maintain a desired relative speed and spacing between the EV pair to sustain cable assembly or stable wireless charging.

The above examples illustrate that this synchronization control work on a traffic scenario different from most others explored by existing cooperative driving algorithms. More exactly, it considers that two designated CAVs initially separated by other vehicles (CAVs or HDVs) and very likely in different lanes want to cooperatively and quickly catch up with each other and then keep a stable and efficient car-following mode. Consequently, the synchronization control is not a simple combination of lane-changing and car-following control. Still, it emphasizes a quick catch-up between two designated CAVs, which differentiates this study from other existing cooperative lane-change and car-following control since they can handle part of the movements in synchronization control, but not the entire synchronization process (Li et al., 2022b; Rios-Torres and Malikopoulos, 2016; Wang et al., 2018), or focusing on a quick catch-up.

Moreover, synchronizing two CAVs' movements will affect their neighbor vehicles and even distant upstream traffic. For example, the study by (Woo and Skabardonis, 2021) claimed that CAVs' heavy lane-change maneuvers to form a platoon dropped the capacity when the traffic was not well below capacity. To account for this effect, both the micro- and macro-traffic dynamics should be involved in the synchronization control development. However, either existing platoon formation studies (Čičić and Johansson, 2019; Ganaoui-Mourlan et al., 2021; Li et al., 2022a; Liang et al., 2015; Tuchner and Haddad, 2017) or cooperative lane change and merging studies (Horowitz et al., 2004; Milanés and Shladover, 2014; Rios-Torres and Malikopoulos, 2016) well investigated this hybrid effect.

To the best of our knowledge, most studies in literature either only partially and separately addressed some aspects of synchronization control or studied it under a simple traffic environment. To match the application requirement, we need to advance existing approaches by holistically considering the entire synchronization process under a complicated traffic environment. Our literature review later presents this research gap in detail. This study seeks to bridge the research gap by developing an efficient and optimal synchronization control. It considers that the two subject CAVs are initially separated (i.e., located in a general position) in a mixed flow including both HDVs and CAVs. The synchronization control will generate optimal control laws to guide the two subject CAVs to approach each other smoothly and efficiently without jeopardizing surrounding traffic efficiency and safety. To achieve this research goal, we contribute the following important modeling and mathematical analysis.

First of all, we developed a Model Predictive Control (MPC) model, which repeatedly generates optimal trajectory control laws to guide the movements of the two subject CAVs for this synchronization purpose at each sampling time step according to the initial and predicted system condition in a time horizon. Overall, the MPC involves enhanced features along with new complexity as follows. It is a hybrid model that captures the microscopic vehicle movement dynamics by existing well-accepted models for the subject CAVs, their neighbor CAVs and HDVs, and then adopts the cell transmission model (CTM) to describe macroscopic traffic flow dynamics. The interaction between the microscopic and macroscopic traffic flow dynamics is captured by introducing integer variables into the CTM so that we can count the flow variation in a cell resulting from microscopic vehicle movements. The resulting hybrid micro-macro model enables the MPC to anticipate the congestion effect resulting from the synchronization control laws but makes some formulations involve nonlinearity. Moreover, the lateral movements of subject CAVs will cause non-smooth car-following relationship changes during the control prediction horizon. To capture this phenomenon, we introduce binary variables to track the leading-following relationships between the subject CAVs and their neighbor vehicles. Together, these enhanced features lead to a highly complicated MPC embedded mixed-integer nonlinear program (MINLP-MPC) with multiple objectives and bring new challenges regarding the recursive feasibility analysis, which is essential to the applicability of an MPC.

Next, we mathematically proved the recursive feasibility of the MINLP-MPC in Theorem 1 by taking advantage of the problem's unique structure features. It has been known that proving the recursive feasibility of an MPC involving integer variables is difficult in general since it involves enormous state spaces resulting from the combinations of integer variables. We noticed that the integer variables of the MINLP-MPC developed in this study are highly correlated. This observation helped us shrink the state spaces to limited

scenarios and then rigorously proved recursive feasibility. More importantly, the proof specifies the conditions that render the recursive feasibility, such as the speed limits, the bound on the human driver's reaction time, and the range of control parameters in the CACC scheme that are followed by neighbor CAVs. The analysis results show that these conditions are satisfied in normal traffic and indicate the strong applicability of the developed MPC system.

Last, the synchronization control is inherently multiple objectives factoring in both microscopic synchronization and macroscopic traffic efficiency, each of which is further interpreted into performance metrics involving several measurements. Accordingly, the optimizer of the MINLP-MPC is multi-objective, requiring effective weighting schemes to generate well-balanced optimal control. To this end, this study contributed an adaptive weighting scheme to balance traffic efficiency and synchronization efficiency. More exactly, we noticed that the synchronization process would experience two distinct dynamic states: catch-up state and platooning state, each of which has a different control priority in the elements of the performance matrix. Then, we transferred the multi-objective MPC to a hybrid MPC system consisting of two sequential MPCs to decorrelate the objective items and reduce the weighting complexity. Built upon that, we developed a weighting strategy for each MPC system to adaptively tune the control priorities based on the initial traffic condition at each control time step. The effectiveness of this weighting strategy and the synchronization control is confirmed in the numerical study. Furthermore, we generalized the MINLP-MPC, the hybrid MPC system, and the adaptive weighting schemes to enable multi-vehicle synchronization with a given vehicle order and target lane. The effectiveness of the generalization was validated in the numerical experiments.

This study carried out extensive numerical experiments to validate the effectiveness of the synchronization control under the developed MPC system. First, our experiments show that the adaptive weighting strategy can generate well-balanced control decisions regarding traffic and synchronization performance and outperforms other weighting strategies that have fixed weights. Moreover, we validated the effectiveness of the MPC system for multi-vehicle synchronization based on the generated vehicle trajectories. Finally, we conducted sensitivity tests to analyze the impacts of traffic congestion, CAV penetration rate and CAV communication range on the synchronization control performance. We found that 150 m is a rational communication range to trigger the synchronization control and a longer range leads to minor improvement. Besides, our numerical experiments demonstrate that the synchronization control is more efficient under a low-moderate congestion level and achieves better performance at high CAV penetration (> 50%).

We present this research by the structure as follows. Following the introduction, Section 2 gives a comprehensive literature review and points out the research gaps we try to bridge. Section 3 provides the preliminary problem formulations, assumptions and briefly introduces the MPC system. Section 4 mathematically formulates the moving dynamics of subject CAVs, HDVs, neighbor CAVs and traffic dynamics of upstream traffic. Next, we formally define the multi-objective MPC system in Section 5 and introduce the adaptive weighting strategy. In Section 6, we analyze the recursive feasibility of the MINLP-MPC model in Section 5. Section 7 extends the synchronization control to more-than-two vehicles scenario. Section 8 further conducts numerical experiments to validate the applicability and effectiveness of our approaches. The entire study and future work are summarized in Section 9.

2. Literature review

In recent decades, spurred by the development of CAV technologies, extensive studies have investigated various CAV cooperative driving algorithms for different traffic scenarios. This section will first recognize those relevant studies and then differentiate our study from these existing efforts, including the cooperative adaptive cruise control (CACC) (Badnava et al., 2021), cooperative lane change and merging control (Vahidi and Sciarretta, 2018), and platoon formation (Ganaoui-Mourlan et al., 2021; Liang et al., 2015; Tuchner and Haddad, 2017). Furthermore, considering the MPC integrates micro- and macro- traffic dynamics to account for the comprehensive traffic impact of motion control, we will also review the recent efforts in hybrid model development (Pasquale et al., 2018; Piacentini et al., 2019a, 2019b, 2018). Along with this review, we will highlight the research gaps and challenges which motivate this study.

First of all, the synchronization control is mainly relevant to adaptive cruise control (ACC) and cooperative adaptive cruise control (CACC). ACC controller manages the brake and throttle to control the acceleration of the vehicle based on the driving information of the preceding vehicle. Its capability is further enhanced with the addition of vehicle-to-vehicle (V2V) communication, leading to CACC. CACC exchanges more extensive information with multiple preceding vehicles and cooperatively optimizes the driving profile which makes the driving process more stable. Existing studies have developed extensive CACC schemes with various control methods, such as proportional integral derivative control (PID) (Knights et al., 2018), sliding mode control (SMC) (Xiao and Gao, 2011; Yan et al., 2017), and model predictive control (MPC) (Kianfar et al., 2015; Maxim et al., 2017; Negenborn and Maestre, 2014), to regulate spacing and speeds of two adjacent CAVs, aiming to mitigate congestion and energy consumption while keeping the vehicle-string stable (Dey et al., 2015; Vahidi and Sciarretta, 2018; Wang et al., 2018). These controllers are either based on the constant distance (CD) policy (Peters et al., 2014), where the inter-vehicle distance is constant and independent of the vehicle's velocity or the constant time headway (CTH) policy (Alsuhaim et al., 2021; Naus et al., 2010), where the inter-vehicle distance varies with the vehicle's velocity. It should be noted that the core of an ACC or a CACC system is a vehicle-following control model, which assumes that the two CAVs are well-positioned in a leading and following relationship without other vehicles in-between. Accordingly, they mainly focus on longitudinal movement control and ignore the lateral movement, which is necessary for the synchronization control in this study.

While considering CAVs' lateral movement, we recognized that many algorithms had been developed to assist cooperative lane-changing and car-following maneuvers. More exactly, optimal lane change decisions can be made in a distributed manner (Nie et al., 2016) or in a centralized framework (Cao et al., 2015), through game models (Talebpour et al., 2015; Wang et al., 2015; Zimmermann et al., 2018), model predictive control approaches (Cao et al., 2015; Liu et al., 2018; Liu and Özgüner, 2015; Zhang et al.,

2022), or other methods (Awal et al., 2015; Balal et al., 2016; Choi and Yeo, 2017; Gong and Du, 2016). These studies are mainly developed for two field applications: (1) platoon merging and splitting maneuvers, in which a CAV conducts lane change to join or leave the platoon (Horowitz et al., 2004; Hu et al., 2020; Li and Li, 2022; Milanés et al., 2010); (2) cooperative car-following and lane-changing CAVs into a target lane (Li et al., 2022b; Li et al., 2020; Ni et al., 2020; Rios-Torres and Malikopoulos, 2016). A comprehensive survey can be found in Li et al. (2022a); Rios-Torres and Malikopoulos (20160; Wang et al. (2018). We noticed that these studies usually either assumed a pure CAV or a CAV-and-HDV mixed environment, in which all CAVs, but HDVs are under the control of the lane change or merging control algorithms. Unlike all these related studies, the synchronization control added one more layer of complexity. It considered at least three types of vehicles under different driving control mixed in the traffic flow, including the two designated subject CAVs following the synchronization control, other CAVs following certain car-following control, and HDVs. From a methodology point of view, these existing studies mainly developed decentralized approaches, which assumed each vehicle adjusted its movement by responding to the perceptions of the neighbor environment rather than pursuing a systematic objective. This is different from the synchronization control, which is developed as a centralized control seeking to cooperatively and optimally synchronize the movement of two CAVs while minimizing the traffic impact on not only the neighbor vehicles but also the distant upstream traffic. Last, most cooperative car-following and lane-changing control did not emphasize the two designated CAVs' catch-up behavior, which is a unique feature of vehicle synchronization, Specifically, vehicle synchronization seeks to have one designated CAV quickly catch up with the other designated CAV while maintaining traffic efficiency. Consequently, existing cooperative car-following and lane-changing algorithms cannot fully address the synchronization control. This new research challenge calls for new methodology development.

The synchronization control is also closely relevant to the recent studies of platoon formation. Specifically, platoon formation solution often follows a three-step framework according to a comprehensive literature review by Li et al. (2022a). They are the protocol design to identify the target platooning lane and vehicle sequence, the trajectory planning, and then vehicle control to generate the location/speed/acceleration of vehicles to form a platoon. From this perspective, the synchronization control fits in the second step of trajectory planning but has a different control objective as mentioned above. Moreover, the main body of platoon formation studies developed a decentralized approach (Bang and Ahn, 2017; Goli and Eskandarian, 2020; Hidalgo et al., 2021; Li et al., 2021, 2022b, 2019; Y. Li et al., 2020; Raboy et al., 2021), while the synchronization control of this study used centralized control. Among the centralized platoon formation studies, some research investigated platoon formation on a single lane. Therefore, lateral movement control is not considered (Čičić and Johansson, 2019; Liang et al., 2015), which is required in the synchronization control. Other studies worked on multilane platoon formation but assumed a pure CAV environment and missed the complexity of the traffic environment (Firoozi et al., 2021; Ganaoui-Mourlan et al., 2021; Graffione et al., 2020; Li and Li, 2022; Tuchner and Haddad, 2017; Zhuang et al., 2020) (Firoozi et al., 2021; Ganaoui-Mourlan et al., 2021). We also noticed that the traffic impact of platoon formation was considered in some protocol designs (Maiti et al., 2019; Woo and Skabardonis, 2021) but barely explored in the trajectory planning/vehicle control steps. In contrast, this study systematically factored the impact of the synchronization control on/from surrounding traffic and distant traffic in the control objective. Therefore, we claim that existing platoon formation algorithms won't work efficiently for the applications with such synchronization requirements since they were developed for different control objectives and could only partially accomplish the synchronization control at some steps or under simplified traffic environments.

Last, the above review indicated that most existing cooperative driving algorithms/models mainly emphasized CAVs' driving safety and efficiency but ignored their impacts on the macroscopic traffic in a broad range. Having recognized this issue, Zhang et al., 2022 developed a platoon-based cooperative lane-change controller that factors the impact on a long-stretch platoon in the target lane. However, if not properly designed, the synchronization control may inevitably affect CAVs' neighborhoods and upstream traffic safety and efficiency significantly. For example, if the synchronization control is too aggressive, it will make CAVs conduct frequent and improper lane change maneuvers. Consequently, it will lead to significant traffic fluctuations in CAVs' local traffic environment. This negative effect will further generate backward shockwaves and propagate backward to affect upstream traffic. Therefore, the synchronization control must co-consider microscopic and macroscopic traffic flow dynamics. Even though such complicated micro-macro traffic flow dynamics is barely considered by existing studies of CAV cooperative driving, they have been integrated into some traffic flow control (Pasquale et al., 2018; Piacentini et al., 2019a, 2019b, 2018). Specifically, these studies considered a CAV platoon as a moving bottleneck (MB). Then, by manipulating CAVs' traffic speed, they imposed variable speed limit (VSL) schemes on other vehicles to mitigate macroscopic congestion. To capture macroscopic traffic response to the VSL, the studies of Piacentini et al. (2018, 2019a, 2019b) introduced an Ordinary Differential Equation (ODE) to couple the MBs' longitudinal movement with the LWR model. To be noted, the proposed synchronization control involves lane-changing movements. Therefore, we need more new approaches to capture the impacts of CAVs' longitudinal and also lateral movements on macroscopic traffic flow.

In short, the synchronization control enables some particular tasks for which we want to efficiently bring two CAVs close to each other and well position them in a stable leading-following mode. There are many such applications when transportation systems widely use CAVs in the future. Those unique features make it different from most existing traffic scenarios that have been investigated by the current CAV cooperative driving control. This study is motivated by viewing the above application needs and research gaps. Below we provide our methodology development and analysis in detail.

3. Problem formulation

Formally, this study considers two subject CAVs are driving in a mixed traffic flow involving both HDVs and CAVs on a freeway segment between two intersections or two ramps. Fig. 1 shows an example. While HDVs follow adjacent vehicles according to humans' response to nearby traffic, CAVs are under certain cruise control such as the CACC scheme. These two subject CAVs, once within a

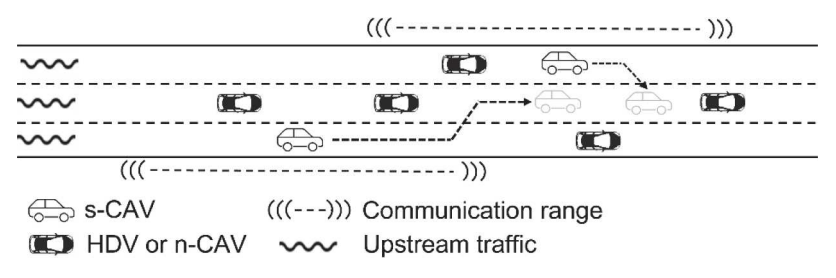


Fig. 1. Pairing two CAVs to a platoon in a mixed traffic environment.

communication range, ¹ will trigger a synchronization control to complete a special task, which requires the following subject CAV to approach the leading subject CAV and then pair to a short platoon efficiently. The special task can be on-the-move EV energy transfer (Abdolmaleki et al., 2019), patrol activities (Hallmark et al., 2019; Subedi et al., 2020), or early period of platoon formation as we mentioned in the introduction. The synchronization control seeks to generate optimal control laws for the two subject CAVs so that they can synchronize their movements smoothly and efficiently without jeopardizing surrounding traffic's efficiency and safety. One of the key challenges to the development of such synchronization control is modeling the interaction between the subject CAVs and the surrounding traffic. More exactly, we cannot control every vehicle for this special task. The surrounding traffic is dynamic and involves various uncertainty. To make the problem tractable, we scope the surrounding traffic of the two subject CAVs from two aspects: (i) a vehicle fleet consisting of neighboring HDVs and CAVs within the subject CAVs' monitoring range, for which we can predict their microscopic movements, and (ii) an adjacent upstream macroscopic traffic segment, for which we can only estimate the traffic propagation. Built upon that, we develop a model predictive control (MPC), which generates optimal discrete trajectory control for the two subject CAVs to efficiently pair to a platoon without worsening the hybrid traffic environment. To mathematically formulate this problem, we introduce the following notations and specifications.

We specify a straight roadway with L number of lanes. The MPC will generate the trajectory control law for the two subject CAV at discrete sampling time steps $t \in \mathbb{Z}_+ := \{0,1,2,\ldots\}$ with a uniform time interval as $\delta > 0$. We label the two subject CAVs by the indices, $i \in I = \{1,2\}$, where i=1 or 2 represents a leading or following subject CAV. Vectors $z_i(t), v_i(t), u_i(t)$ denote the position, speed, and control input (acceleration/deceleration) of the subject CAV i in longitudinal x and latitudinal y directions at time step t, respectively. Namely, $z_i(t) = [x_i(t), y_i(t)]^T$, $v_i(t) = [v_i^x(t), v_i^y(t)]^T$, and $u_i = [u_i^x(t), u_i^y(t)]^T$, i=1,2. The two subject CAVs are able to monitor the movements of their neighboring vehicles $\omega \in \Omega$ within the communication range, which can be either HDVs defined as the set Ω_h or CAVs defined as the set Ω_c running in different lanes (we have $\Omega = \{\Omega_c, \Omega_h\} = \{\Omega_c^l, \Omega_h^l\}_{l=1}^L$). Specifically, we denote $\widehat{x}_\omega(t)$ and $\widehat{v}_\omega(t)$ as the position and speed of a neighboring vehicle ω , $\forall \omega \in \Omega$. To differentiate subject CAVs and their neighboring CAVs, we denote a subject CAV as s-CAV, and a CAV in the neighborhood of the subject CAVs as n-CAV throughout the rest of the paper. We also consider a vehicle set $J = I \cup \Omega$, which consists of all s-CAVs and their neighbor vehicles (n-CAVs and neighbor HDVs).

Given that the latitudinal movements of s-CAVs will change their lane positions and then affect the following behavior of their neighboring vehicles, we thus introduce binary variables $\gamma_j^l(t)$, $\rho_{j,j'}^l(t)$ and $\eta_{j,j'}^l(t)$ in (1) - (3) to capture the state change resulting from this vehicle movement dynamics.

$$\gamma_j^l(t) = \begin{cases} 1 & \text{if vehicle j run in lane l at time step t} \\ 0 & \text{otherwise} \end{cases}, \ \forall j \in J, \ l \in L$$
 (1)

$$\rho_{j,j'}^l(t) = \begin{cases} 1 & \text{if vehicle j' is downstream to vehicle j in lane 1 at time step t} \\ 0 & \text{otherwise} \end{cases}, \ \forall j, \ j' \in J, \ l \in L$$

$$\eta_{j,j'}^l(t) = \begin{cases} 1 & \text{if vehicle j follows j}' \text{ in lane 1 at time step t}, \ \forall j, \ j' \in J, \ l \in L \\ 0 & \text{otherwise} \end{cases}$$
 (3)

Mainly, $\gamma_j^l(t)$ indicates if a vehicle j is running in a lane l at a time step t. $\rho_{j,j'}^l(t)$ demonstrates if vehicle j' is running downstream to vehicle j and $\eta_{j,j'}^l(t)$ specifies if vehicle j is an immediate follower of vehicle j'. We determine the variable $\gamma_j^l(t)$ based on the latitudinal coordinate $y_j(t)$ of vehicle j by the logical condition (4), where $\left[\underline{y}^l,\overline{y}^l\right]$ is the latitudinal boundary coordinates of lane l.

$$\gamma_j^l(t) = \left[\underline{y}^l < y_j(t) \le \overline{y}^l \right], \ \forall j, l \in L$$

¹ The V2V communication can apply various communication technology, such as cellular (C-V2X) including 5G and LTE, and dedicated short-range communications (DSRC). The communication range for C-V2X and DSRC are up to 500 meters, and 300 meters, respectively, with 100% packet delivery rate. Because the macroscopic traffic impact on distant upstream traffic flow is considered, it is not necessary to consider a long communication range to trigger the synchronization control (see the sensitive test later).

Clearly, there exists a logical relationship between $\gamma_j^l(t)$ and $\rho_{j,j'}^l(t)$, $\forall j,j' \in J$. For example, $\rho_{j,j'}^l(t) = 1$ if and only if both j and j' are in the same lane, i.e., $\gamma_j^l(t) = \gamma_j^l(t) = 1$, and vehicle j' is in the downstream of vehicle j, i.e., $x_j(t) < x_{j'}(t)$. This logical condition is represented in (5), where \wedge represents the logical relationship: "and". The logical conditions (5) can be molded as a set of integer constraints in the Appendix A.

$$\rho_{i,l}^{l}(t) = \left[x_{j}(t) < x_{j}^{l}(t)\right] \wedge \gamma_{j}^{l}(t) \wedge \gamma_{l}^{l}(t), \ \forall j,j' \in J, l \in L$$

$$\tag{5}$$

Built upon $\rho_{jj}^l(t)$, we can determine the value of $\eta_{jj}^l(t)$ based on the logical condition in (6). Mainly, we can tell that vehicle j is following vehicle j' at time t on lane l (i.e., $\eta_{j,j}^l(t)=1$), if and only if two conditions are satisfied: (i) vehicle j' is in the downstream of vehicle j ($\rho_{j,j}^l(t)=1$) and (ii) there are no vehicles between them (i.e., $[\sim \rho_{j,k}^l(t)] \land [\sim \rho_{k,j}^l(t)]$, $\forall k\neq j$ and $k\neq j'$). Here, the symbol " \sim " represents the "not" operation. This logic relationship can be further modeled by integer constraints given in the Appendix A.

$$\eta_{j,j'}^l(t) = \rho_{j,j'}^l(t) \wedge \bigcap_{k \in J/\{j,j'\}} \left\{ \left[\sim \rho_{j,k}^l(t) \right] \wedge \left[\sim \rho_{k,j'}^l(t) \right] \right\}, \forall j,j' \in J, \ l \in L$$

$$\tag{6}$$

Besides the *s*-CAVs and their neighboring vehicles (HDVs and *n*-CAVs), the synchronization control also considers the flow dynamics of the upstream traffic outside of the monitoring range of *s*-CAVs. To do that, we discretize the highway segment without intermediate entrances or exits into *C* number of cells for each lane $l \in L$. Each cell has length ΔL . According to Courant-Friedrichs-Lewy condition, the conservation law holds only when $\Delta L \geq \delta v_f$ (Daganzo, 1995). Each cell c = 1, 2, ..., C at a time step t = 1, 2, ..., T is associated with the traffic characteristics as follows. $\int_c^l (t)$: the traffic flow of cell *c* in lane l [veh/h]; $\int_c^l (t)$: entering flow to cell *c* from cell c - 1 in lane l [veh/h]; $\int_c^l (t)$: sending flow from *c* to cell c + 1 [veh/h] in lane l; $r_c^l(t)$: receiving flow of cell *c* from cell c - 1 in lane l (receiving flow) [veh/h].

The sections below will introduce the microscopic vehicle dynamics, the macroscopic traffic dynamics, and their interaction. Built upon that, we developed the MPC for this synchronization control.

4. Microscopic and macroscopic traffic dynamics

The synchronization control will generate the trajectory control law for the s-CAVs while predicting the moving dynamics of neighbor vehicles, i.e., n-CAVs and neighboring HDVs, as well as the upstream traffic propagation. This section develops mathematical formulations to capture the corresponding microscopic and macroscopic traffic dynamics. To be noted, the latitudinal movements of s-CAVs enable lane-change behaviors. It raises the difficulties in formulating the traffic dynamics of its neighboring vehicles and upstream traffic. We address those challenges in the following subsections. Note that the microscopic and macroscopic traffic dynamics are both updated with a timestep size equal to the control time interval δ .

4.1. Subject CAVs dynamics

The movements of the s-CAVs are subject to the longitudinal and latitudinal dynamics as well as several important states and control constraints. More exactly, we describe the longitudinal and latitudinal dynamics of the s-CAVs by the well-accepted double-integrator model in (7) and (8) (Nilsson et al., 2016, 2015; Tomas-Gabarron et al., 2013; Wang et al., 2019).

$$z_i(t+1) = z_i(t) + \delta v_i(t) + \frac{\delta^2}{2} u_i(t), \ \forall i \in I$$

$$(7)$$

$$v_i(t+1) = v_i(t) + \delta u_i(t), \ \forall i \in I$$
(8)

where $z_i(t), v_i(t), u_i(t)$ represents $z_i(t\delta), v_i(t\delta), u_i(t\delta)$ respectively for notational simplicity. Moreover, we consider that the control input $u_i(t)$ and speed $v_i(t)$ keep constant in each time interval [t, t+1) for $t \in T$, and they are subject to the control and speed limits in (9) and (10).

$$\underline{a} \le u_i(t) \le \overline{a}, \ \forall i \in I$$

$$\underline{v} \le v_i(t) \le \overline{v}, \ \forall i \in I$$
 (10)

Besides, a subject CAV's movement is also subject to the safety distance constraint in (11).

$$x_j(t) - x_i(t) \ge L_i + \tau_i v_i^x(t) - \frac{\left[v_i^x(t) - v_x\right]^2}{2 a_x}, \forall i \in I$$
 (11)

where $x_j(t)$ is the longitudinal position of the leading vehicle j of subject CAV i follows; $\tau_i > 0$ is the constant reaction time due to dynamic and other delays; $L_i > 0$ is a constant depending on vehicle length; \underline{a}_x and $\underline{\nu}_x$ are the minimum possible horizontal acceleration and minimum horizontal speed limitation. Constraint (11) is a conservative safety constraint. It specifies a safety lower bound on the safety spacing and ensures conflict-free driving (Gong et al., al.,2016; Gong and Du, 2018). This safety is suitable for freeway traffic but might be too conservative for urban traffic. It can be adapted for urban traffic by using other safety constraints such as Wang et al.

(2020), (2014); Wu et al. (2020)). It won't affect the applicability of our approach.

Constraint (11) indicates the need to track the longitudinal position (i.e., $x_j(t)$) of s-CAV (i)'s leading vehicle j to keep a safe distance. However, the leading vehicle of a s-CAV can be another s-CAV, a n-CAV, or an HDV and it may switch during the control prediction zone T due to its latitudinal movement. To capture these dynamics, we utilize binary variables $\gamma_i^l(t)$ and $\rho_{i,j}^l(t)$ as defined in and (1) and (2). Specifically, variable $\gamma_i^l(t)$ is introduced to track the lane that the s-CAV(i) is running in, and variable $\rho_{i,j}^l(t)$ monitors its downstream neighbor vehicles. Consequently, we rewrite the safety constraint (11) into constraints (12) and (13), considering two scenarios: (1) s-CAV(i) follows another s-CAV(i) and (2) s-CAV(i) follows a n-CAV or an HDV.

$$x_{i}'(t) - x_{i}(t) \ge L_{i} + \tau_{i}v_{i}^{x}(t) - \frac{\left[v_{i}^{x}(t) - v_{\underline{x}}\right]^{2}}{2 a_{x}} - M\left[3 - \gamma_{i}^{l}(t) - \gamma_{i}^{l}(t) - \rho_{i,i}^{l}(t)\right], \forall i, i' \in I, \ l \in L$$

$$(12)$$

$$\widehat{x}_{\varpi}(t) - x_i(t) \ge L_i + \tau_i v_i^{\mathsf{x}}(t) - \frac{\left[v_i^{\mathsf{x}}(t) - \underline{v}_{\underline{\mathsf{x}}}\right]^2}{2 \ a_{\mathsf{x}}} - M \left[2 - \gamma_i^l(t) - \rho_{i,\varpi}^l(t)\right], \forall \varpi \in \Omega_h^l, \ l \in L, i \in I$$

$$(13)$$

where $\hat{x}_{\varpi}(t)$ in constraint (13) is the longitudinal coordinate of neighboring vehicle ϖ at time interval t. M takes a relatively big value, i.e., the length of the roadway. Constraint (12) is activated when $\gamma_i^l(t) = \gamma_{i'}^l(t) = \rho_{i,i'}^l(t) = 1$, indicating s-CAV(i) follows another s-CAV (i) in the downstream. Constraint (13) is activated when $\gamma_i^l(t) = \rho_{i,\varpi}^l(t) = 1$, indicating when s-CAV(i) follows a neighbor vehicle ϖ (HDV or n-CAV) in the downstream. The two constraints are inactive when s-CAV(i) and neighboring vehicle ϖ is not in the downstream of s-CAV(i).

4.2. HDVs moving dynamics

We consider that neighboring HDVs are not under a trajectory control scheme or our synchronization control. Still, their movements are restrained by their leading vehicles in this local area, thus can be predicted by using Newell's car-following model (14) during the prediction horizon.

$$\widehat{v}_{\omega}(t+k) = \frac{\delta}{\tau_{\omega}} s_{\omega,j}(t) - \frac{\delta d_{\omega}}{\tau_{\omega}} \ \forall \omega \in \Omega_{h}^{l}, l \in L, \ j \in J$$

$$\tag{14}$$

where $s_{\omega,j}(t) = x_j(t) - \widehat{x}_{\omega}(t)$, $j \in J$ represents the spacing with the HDV ω and its leading vehicles j at time step t; τ_{ω} represents the reaction time and d_{ω} represents the minimum stop distance of HDV ϖ . Both τ_{ω} and d_{ω} can be adaptively learned by adopting an online-learning approach (Gong and Du, 2018). τ_{ω} will be rounded to an integer number, and the control step size δ will be selected such that $k = \frac{\tau_{\omega}}{\delta}$ is an integer to fit HDV dynamics into the model. Moreover, to ensure that the HDV reaction happens within a prediction horizon, the control timestep size δ should also satisfy $T \geq \frac{\tau_{\omega}}{\delta}$, which is $\delta \geq \frac{\tau_{\omega}}{T}$.

Please note that (14) does not explicitly identify the HDV's lane. It will be specified when we recognize its leading vehicle j through the logic constraints in (4). Mainly, the leading vehicle j can also be a s-CAV (i), n-CAVs, or HDV ω' . Accordingly, we set $s_{\omega,i}(t) = x_i(t) - \widehat{x}_{\omega}(t)$, if HDV ω is following a s-CAV(i) in the same lane l (i.e., $\rho_{\omega,i}^l(t) = 1$) at time t; otherwise, we make $s_{\omega,i}(t) = M$, which is a sufficiently large number. Similarly, we have $s_{\omega,\omega'}(t) = \widehat{x}_{\omega'}(t) - \widehat{x}_{\omega}(t)$, if HDV ω is following a neighbor vehicle ω' on the same lane at time step t; otherwise, we make $s_{\omega,\omega'}(t) = M$. We formulate the above thoughts in (15).

$$s_{\omega,j}(t) = \begin{cases} x_j(t) - \widehat{x}_{\omega}(t) & \rho_{\omega,j}^l(t) = 1\\ M & \rho_{\omega,j}^l(t) = 0 \end{cases}, \ \forall \omega \in \Omega_h^l, j \in I \cup \Omega^l, l \in L$$
 (15)

where $\rho^l_{\omega,j}$ is defined by (2) and is determined by the logical condition (5). In particular, (15) considers $\rho^l_{\omega,i}(t)$ regarding *s*-CAV(*i*) as a variable because the latitudinal movement of *s*-CAVs will change this following relationship during the control prediction horizon. But, (15) keeps $\rho^l_{\omega,\omega'}(t)$ regarding neighboring HDV(ω') as a given parameter according to the initial condition since we assume that the neighbor HDVs will stay in the same lane during a prediction horizon (see the justification later). Then we identify the following spacing, $s_{\omega,j}(t)$ of HDV ω by Eq. (16), where $s_{\omega,1}(t)$, $s_{\omega,2}(t)$ are spacing between HDV ω and *s*-CAV(1) and *s*-CAV(2).

$$s_{\omega,i}(t) = \min\{s_{\omega,\omega^i}(t), s_{\omega,1}(t), s_{\omega,2}(t)\} \ \forall \omega \in \Omega^i_k, \ l \in L$$
 (16)

Based on (14) to (16), Eqs. (17) and (19) estimate the trajectory profiles of HDVs based on Newell's car-following model. Please note that the Newell's car-following model does not set speed limits as it is mostly applied in congested scenarios. In this study, when the traffic is sparse and the spacing $s_{\omega}(t)$ is large, we consider an upper bound $\overline{v_x}$, i.e., free-flow speed, to the estimated speed to make it consistent with reality. Also, we consider a lower bound v_x to the estimated speed.

$$\widehat{v}_{\omega}(t+k) = \min\left\{\frac{\delta}{\tau_{\omega}} s_{\omega j}(t) - \frac{\delta d_{\omega}}{\tau_{\omega}}, \ \overline{v_{x}}\right\} \forall \omega \in \Omega_{h}^{l}, l \in L$$

$$\tag{17}$$

$$\widehat{v}_{\omega}(t+k) = \max \left\{ \frac{\delta}{\tau_{\omega}} s_{\omega j}(t) - \frac{\delta d_{\omega}}{\tau_{\omega}}, \ \underline{v_{x}} \right\} \ \forall \omega \in \Omega_{h}^{l}, \ l \in L$$

$$(18)$$

$$\widehat{x}_{\omega}(t+k) = \widehat{x}_{\omega}(t) + \frac{\tau_{\omega}}{\delta}\widehat{v}_{\omega}(t), \ \forall \omega \in \Omega_{h}^{l}, l \in L$$

$$\tag{19}$$

Finally, HDVs are also subject to the safety distance constraint when the s-CAV cuts in front of the HDV. Let us consider a scenario where the s-CAV(i) travels at the speed v_{ω}^{x} and cuts in front of the HDV who travels faster at the speed \widehat{v}_{ω} , i.e., $\widehat{v}_{\omega} > v_{\lambda}^{x}$. Given that the HDV needs time τ_{ω} to react to the lane change of s-CAV(i), it is necessary to specify the lane-change conditions for s-CAV(i) to avoid the collision. Specifically, we require s-CAVs to satisfy the following conditions to cut in front of an HDV. They are derived from the safety lane-change constraints in Chen et al. (2013) (see Section 6 for details).

$$x_{i}(t) - \widehat{x}_{\omega}(t) \ge d_{\omega} + \frac{\tau_{\omega}}{\delta} \widehat{v}_{\omega}(t) - M \left(1 - \eta_{\omega,i}^{l}(t) + \eta_{\omega,i}^{l}(t-1) \right) \ \forall \omega \in \Omega_{h}^{l}, l \in L, i \in I$$

$$v_i(t) - \widehat{v}_{\omega}(t) \ge -M \left(1 - \eta_{\omega,i}^l(t) + \eta_{\omega,i}^l(t-1) \right) \ \forall \omega \in \Omega_h^l, l \in L, i \in I$$

where $\eta^l_{\omega,i}(t)$ is defined by (3) and is determined by the logical condition (6). In particular, when the *s*-CAV(*i*) cuts in front of HDV(ω) at time step t ($\eta^l_{\omega,i}(t)=1$ and $\eta^l_{\omega,i}(t-1)=0$), constraint (20) is activated such that the spacing between *s*-CAV(*i*) and HDV(ω) needs to no smaller than the safety distance $d_\omega+\tau_\omega\widehat{\nu}_\omega(t)$. Also, the speed of *s*-CAV(*i*) needs to no less than that of HDV(ω) indicated by constraint (21).

Note that the assumption that the neighbor HDVs stay in the same lane during the prediction horizon is valid for our MPC introduced in the later section. Briefly, MPC is a feedback control. At each control sampling time step, it takes the new initial condition of the system as input and generates the control law for the system in multiple steps but only implements the first step. Therefore, if a lane change occurs during a prediction horizon, the correction will be built in the next time step as we recompute the control law by resetting the initial conditions in the MPC. This assumption also makes Eq. (16) valid because ω' is defined as the leading vehicle of HDV ω at beginning, during the prediction horizon, the leading vehicle of ω can only be ω' or one of the subject CAVs. In addition, we recognized that other advanced car-following models could predict the HDV dynamics. Still, our MPC modeling adopted Newell's carfollowing model thanks to its linear and friendly format to facilitate the computation. Additionally, the merit of this closed-loop feedback control may also correct prediction errors of Newell model resulting from previous steps. Even though other complicated car-following models, such as Intelligent Driver Model (IDM) (Lu et al., 2018), may give more accurate predictions, they raise high computation and then risk the control continuity (e.g., solving a complicated MINLP within one second). To address those issues, we often must do linearization or approximation that in turn degrades the prediction accuracy. Co-considering the above factors, we think Newell's car-following model is a good fit for this study.

4.3. Neighboring CAVs moving dynamics

Recall that we consider the neighboring CAVs follow certain cruise control schemes, such as CACC. There are many CACC schemes developed in literature (Rahman et al., 2017; Sharath and Velaga, 2020) and we apply a first-order model derived by PATH to model the CACC car-following behavior (Milanés and Shladover, 2014; Qin et al., 2021), since existing field experiments have confirmed its good performance to capture the car-following movement of current commercially available CACC systems. Specifically, the CACC model formulates the vehicle speed by the speed and gap error in the previous time step as follows,

$$\widehat{v}_{\omega}(t+1) = \widehat{v}_{\omega}(t) + k_1 e_{\omega}(t+1) + k_2 \dot{e}_{\omega}(t+1) \ \forall \omega \in \Omega^l_{\epsilon}, \ l \in L$$

$$(22)$$

where ω is the neighbor CAV and control gains k_1 and k_2 are set as 0.01 s^{-2} and 1.6 s^{-1} (Xiao et al., 2017); $\dot{e}_{\omega}(t)$ is the derivative of the gap error defined in (24). Here, we set the update timestep size of the CACC scheme for neighboring CAVs to be the same as the *s*-CAV's control timestep size, δ .

$$e_{\omega}(t) = \hat{x}_{l}(t) - \hat{x}_{\omega}(t) - t_{d}\hat{v}_{\omega}(t) \ \forall \omega \in \Omega_{c}^{l}, \ l \in L$$
 (23)

The derivative of gap error is defined in (24).

$$\dot{e}_{\omega}(t) = \hat{v}_{j}(t) - \hat{v}_{\omega}(t) - t_{d}a_{\omega}(t) \ \forall \omega \in \Omega_{c}^{l}, \ l \in L$$

$$\tag{24}$$

where vehicle j is the leading vehicle of the neighbor CAV ω , t_d is the desired time gap of the CACC controller, which is set to 0.6s; $a_{\omega}(t)$ is the acceleration of CAV ω at time step t, which is represented by $\frac{\widehat{V}_{\omega}(t+1)-\widehat{V}_{\omega}(t)}{\Delta t}$. Combined Eqs. (22), (24) and (24), we represent the speed of CAV ω by the speed of ϖ and leading vehicle j at previous time step and its spacing with the leading vehicle, $s_{\omega,j}(t)$.

$$\widehat{v}_{\omega}(t+1) = A\widehat{v}_{\omega}(t) + B\widehat{v}_{j}(t+1) + Cs_{\omega,j}(t+1) \ \forall \omega \in \Omega_{c}^{l}, l \in L, \ j \in J$$

$$\tag{25}$$

 $^{^{2}}$ If the leading vehicle of ω is a s-CAV at beginning of prediction horizon, then ω' is defined as the nearest HDV or the *n*-CAV in the downstream.

where
$$A = \frac{\delta(1-k_1t_d-k_2)+k_2t_d}{\delta+k_2t_d}$$
, $B = \frac{\delta k_2}{\delta+k_2t_d}$, $C = \frac{\delta k_1}{\delta+k_2t_d}$

where $A = \frac{\delta(1-k_1t_d-k_2)+k_2t_d}{\delta+k_2t_d}$, $B = \frac{\delta k_2}{\delta+k_2t_d}$, $C = \frac{\delta k_1}{\delta+k_2t_d}$. Again, due to the lateral movement of *s*-CAVs, the leading vehicle of a *n*-CAV can also be a *s*-CAV, an HDV or another *n*-CAV, and it may vary at each time step during the control horizon. Then to implement Eq. (25) in our MPC, we also need to recognize the leading vehicle and their trajectory for each n-CAV at each time step. Thus, we utilize binary variables, $\eta_{\omega,\alpha'}^l(t)$, $\eta_{\omega,1}^l(t)$ and $\eta_{\omega,2}^l(t)$ defined in (3) to help. Specifically, $\eta^l_{\omega,\omega'}(t)=1$, if the leading vehicle of n-CAV(ω) is vehicle ω' (HDV or n-CAV); otherwise $\eta^l_{\omega,\omega'}(t)=0$. $\eta^l_{\omega,i}(t)=1$, if the leading vehicle of n-CAV(ω) is a s-CAV at time step t; otherwise $\eta_{\omega,i}^l(t)=0$. Consequently, Eq. (25) is reformulated to (26) for adapting it to this study.

$$\widehat{v}_{\omega}(t+1) = A\widehat{v}_{\omega}(t) + B\eta_{\omega,\omega'}^{l}(t)\widehat{v}_{\omega'}(t) + B\sum_{i \in I} \eta_{\omega,i}^{l} v_{i}^{x}(t) + Cs_{\omega}(t), \ \forall \omega \in \Omega_{c}^{l}, l \in L$$

$$(26)$$

where, $s_{\omega,j}(t)$ is captured by Eq. (16) also, but only for $\omega \in \Omega^l_c$ and $\eta^l_{\omega,j}(t)$ is identified by the logical condition defined in (6).

Finally, we also require s-CAV to satisfy the following lane-change condition (27) to cut in front of an n-CAV without collision (see Section 6 for a detailed derivation). Note that most of the safety lane-change constraints are designed for the lane-change vehicle that cuts in front of an HDV, which cannot be applied to this scenario where the following vehicle in the target lane is another CAV following a CACC control.

$$v_i^{\mathsf{x}}(t) - \widehat{v}_{\omega}(t) \ge \frac{\widetilde{a}_i(t-1)\delta\left(B - \frac{1}{2}\right)}{A} - M\left(1 - \eta_{\omega,i}^l(t) + \eta_{\omega,i}^l(t-1)\right) \ \forall \omega \in \Omega_c^l, l \in L, i \in I$$

where $\widetilde{a}_i(t-1) = max \Big[\underline{a}_x, a_{i,v}(t-1)\Big]$, and $a_{i,v}(t-1) = \frac{v_x - v_t^x(t-1)}{\delta}$. When s-CAV cuts in front of the n-CAV, i.e., $\eta_{\omega,i}^l(t) = 1$ and $\eta_{\omega,i}^l(t-1)$ = 0, constraint (27) is activated and ensures that the s-CAV should cut-in with enough speed to avoid the collision.

To be noted, our MPC modeling is not limited to the CACC scheme developed by PATH. It can accommodate various existing CACC schemes, even though they may affect the algebra discussions of recursive feasibility proof discussed in Section 6. More importantly, we surmise that different CACC schemes will bring common benefits to synchronization control thanks to their common merits in the following aspects. First, they usually enable CAVs to keep a smaller space while an s-CAV cuts in front. Second, they will allow CAVs to drive cooperatively, making lane-change of s-CAV smoother. Those two inherent features of various CACC schemes help improve the overall efficiency and smoothness of the synchronization control. We conduct experiments to confirm this point (see Appendix D).

4.4. Flow dynamics

The synchronization control will instruct subject CAVs to speed up or slow down, and perform overtaking or lane-change maneuvers so that these two CAVs can approach each other efficiently. However, these maneuvers may harm upstream surrounding traffic. To capture this effect, we will extend standard CTM to describe traffic propagation corresponding to the synchronization control, namely, the interaction between the macroscopic upstream traffic and microscopic subject CAVs/neighbor vehicles' movement. The update timestep size for CTM is selected as the same as MPC control timestep size, δ . It is valid as long as the cell length ΔL and timestep size δ satisfy the Courant-Friedrichs-Lewy condition, $\Delta L \ge \delta \nu_f$. For completeness, we present the CTM in constraints (28) -(31), which capture flow propagation among cells in general. Note that we develop CTM on each lane on the road segment of interest.

$$\int_{c}^{l} (t+1) = \int_{c}^{l} (t) + y_{c}^{l}(t) - y_{c+1}^{l}(t), \forall c \in C_{l}, l \in L$$
(28)

$$y_c^l(t) = \min\{s_{c-1}^l(t), r_c^l(t)\}, \ \forall c \in C_l, l \in L$$
 (29)

$$J_{\epsilon}(t) = \min\{ \mathcal{N}_{\epsilon}(t), q_{\epsilon}^{l,max} \}, \forall \epsilon \in C_l, l \in L$$

$$(30)$$

$$\nu_c^l(t) = \min\{w_c^l(k_c^{l,max} - k_c^l(t)), \ q_c^{l,max}\}, \ \forall c \in C_l, l \in L$$
(31)

where $q_c^{l,max}$ is the capacity of the cell c in lane l, w_c^{l} is the congestion wave speed and $k_c^{l,max}$ is the jam density. $k_c^{l}(t)$ is the density of cell c in lane l on time interval t. Note that we develop CTM on each individual lane on the road segment of interest.

For a cell *c* at time step *t*, constraints (28) is the flow conservation constraint. Namely, the cell *c*'s flow at time step t+1, $\int_{c}^{t} (t+1)$, is equal to the cell's flow at time step t, $\int_c^t (t)$, plus the flow propagation occurring during the time interval from t to t+1 (i.e., plus the flow entering to this cell from an upstream cell, $g_c^l(t)$, and minus the flow leaving from this cell for its downstream cell, $g_{c+1}^l(t)$ at time step t). Constraint (29) limits that at time step t, the entering flow to cell c from an upstream cell c-1 is given as the minimum value of the sending flow from its upstream cell c-1, $J_{c-1}(t)$, and its receiving flow $r_c^l(t)$ at time step t. For a given cell c at a time step t, the sending flow $J_c(t)$ is limited by the minimum flow that the cell has and its flow capacity. Constraint (31) further models the receiving flow $r_c^l(t)$, which is the minimum flow of the cell c' capacity and its rest flow capacity at time step t.

Constraints (28) - (31) altogether describe the upstream macroscopic traffic flow dynamics. However, this study is particularly interested in capturing the influence of the individual vehicles under the synchronization control or monitoring, i.e., s-CAVs ($i \in I$) and their neighbor vehicles ($\omega \in \Omega$), on the upstream flow propagation. Specifically, the interactions between those individual vehicles and

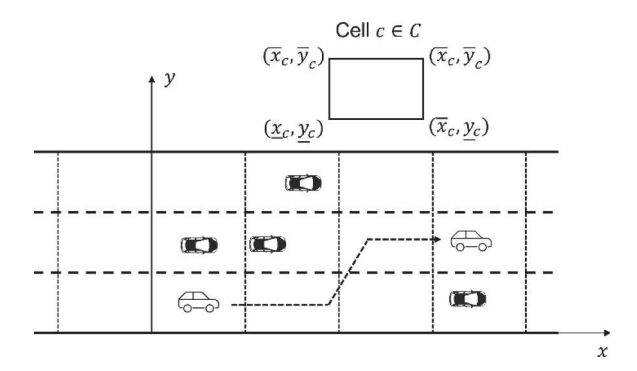


Fig. 2. Roadway representation in CTM.

macroscopic upstream traffic first occur in boundary cells where they are mixed. For these cells, the entering (or leaving) of those individual vehicles ($\in I$ or $\omega \in \Omega$) increases (or reduces) the rest flow capacity of the cell and limits the upstream flow propagation from upstream cells. For example, when the deceleration of a subject CAV slows down its following neighbor vehicles in a cell c, the corresponding density, $k_c^l(t)$ will increases. The increased cell density will reduce the receiving flow $c_c^l(t)$ from its upstream cell according to constraint (31), which further reduces the entering flow to the cell $c_c^l(t)$ by constraint (29). As a result, the movement of the subject CAVs will affect the upstream traffic flow in the cell in the next time step $c_c^l(t+1)$ and cause congestion.

To model the interaction between the microscopic and macroscopic traffic flow dynamics, we need to recognize the boundary cells that s-CAVs, n-CAVs and neighbor HDVs belong at each time step. With cell length ΔL , we locate the coordinates for each cell by $\overline{z}_c^l = (\overline{x}_c^l, \overline{y}_c^l)$ and $\underline{z}_c^l = (\underline{x}_c^l, \underline{y}_c^l)$ as Fig. 2 shows. Based on these coordinates, (32) and (33) specify the criteria to find the cells involving subject CAVs and neighboring vehicles. Specifically, the binary variable $\phi_{i,c}^l(t)$ takes value one when the coordinates of subject CAV(i), $z_i(t)$, fall within the cell c in lane l at time t, and 0 otherwise. Similarly, $\phi_{\omega,c}^l(t)$ takes value one when the coordinates of neighbor vehicle ω , $\widehat{x}_{\omega}(t)$, fall within the cell c in lane l at time t, and 0 otherwise. Moreover, we have constraint (34) to ensure that each vehicle can only be present in one cell at a time. Eq. (35) gives the formulation to calculate traffic density $k_c^l(t)$ in a cell. To be noted, it counts both aggregated flow and individual vehicles with trajectory control or estimation in this study. Thus, by combining CTM in (28) - (31) with the cell membership recognition in (32)-(34), (35) can capture the interaction between macroscopic and microscopic traffic dynamics. The logic functions in (32) and (33) can be further transferred to integer constraints given in Appendix A.

$$\phi_{l,c}^{l}(t) = \left[z_{i}(t) \geq z_{c}^{l} \wedge \left[z_{i}(t) < \overline{z}_{c}^{l}\right], \ \forall \ i \in I, c \in C_{l}, l \in L\right] \tag{32}$$

$$\phi_{\omega,c}^{l}(t) = \left[\widehat{x}_{\omega}(t) \ge \underline{x}_{c}^{l}\right] \wedge \left[\widehat{x}_{\omega}(t) < \overline{x}_{c}^{l}\right], \ \forall \omega \in \Omega^{l}, \ c \in C_{l}, l \in L$$
(33)

$$\sum_{l=1}^{L} \sum_{c=1}^{C} \phi_{j,c}^{l}(t) = 1, \ \forall j \in J$$
 (34)

$$k_c^l(t) = \mathcal{I}_c^l(t) + \sum_{j \in I} \phi_{j,c}^l(t) / \delta \Delta L, \ \forall c \in C_l, l \in L$$

$$(35)$$

5. MPC for synchronization control

According to the control theory in Rawlings et al. (2017), MPC is based on iterative, finite-horizon optimization of a dynamic system. More exactly, at time t the current system state is sampled, and a cost/error minimizing control strategy is computed for a relatively short time horizon in the future [t,t+T] with uniform time interval. Only the first step of the control strategy is implemented, then the system state is sampled again, and the calculations are repeated starting from the new current state, yielding a new control and new predicted state path. In the context of synchronization control, MPC takes current upstream traffic's and vehicles' states (both s-CAVs and neighboring HDVs and CAVs) as inputs, predicts their future states in T time steps by vehicle/traffic dynamics models, and then generates the optimal control law for s-CAVs in T steps, but only implements the first step, by solving an optimization model. This recursive process will reset the surrounding traffic condition by recognizing new neighbor vehicles and their trajectory profiles at each control sampling step. To a certain extent, it will address the issues regarding prediction error and traffic uncertainty in control. Therefore, it fits this study very well. The MPC built for this study involves a mixed-integer optimizer with multiple objectives to generate the optimal trajectory control law co-considering synchronization and traffic efficiency. By noticing the complexity of weighting control objectives, we further transfer it to two sequential MPCs according to the problem features. Built upon that, we develop an adaptive weighting strategy for balancing the synchronization and traffic efficiency under different states. Below we introduce the technical details for the model development and analysis.

Table 1Objective items and corresponding weights.

Objective item (weight)	Explanation	
Traffic performance metric		
	$J_w(Q_w)$	Featuring traffic efficiency by s-CAVs' speed.
	$J_{_{\mathscr{Y}}}\left(Q_{_{\mathscr{Y}}} ight)$	Featuring traffic efficiency by upstream flow propagation.
Synchronization performance metric	$J_{\eta} \; (Q_{\eta})$	Featuring synchronization efficiency by two s-CAVs' positions (in car-following mode)
	$J_{\sigma}\left(Q_{\sigma}\right)$	Affecting speed harmonization by the relative speed of the two s-CAVs.
	$J_{z}\left(q_{z}\right)$	Featuring synchronization efficiency by the relative spacing of s-CAVs.

5.1. Multi-objective MPC and a hybrid MPC system

The MPC for the synchronization control takes the initial states of s-CAVs, n-CAVs and the upstream traffic as inputs at time step $t \in \mathbb{Z}^+$, and then seeks to generate the optimal control law to instruct subject CAVs' trajectories at t+1 so that they can approach each other and synchronize their motion efficiently without jeopardizing traffic efficiency. The synchronization control is subject to the prediction of s-CAVs' and n-CAVs' movements and the upstream traffic propagation in future T steps according to the micro and macro dynamics introduced in Section 4. The above thoughts are demonstrated by the MPC in (36). Without loss of generality, we make t start with zero in the formulation.

$$J(u_t) = \min \sum_{t=0}^{T-1} \frac{1}{2} \left[\underbrace{u_t^T Q_{\mathbf{u}} u_t}_{J_{\mathbf{u}}} + \underbrace{\mathbf{w}_t^T Q_{\mathbf{w}} \mathbf{w}_t}_{J_{\mathbf{w}}} - \underbrace{\mathbf{y}_t^T Q_{\mathbf{y}} \mathbf{y}_t}_{J_{\mathbf{y}}} - \underbrace{\eta_t^T Q_{\mathbf{y}} \eta_t}_{J_{\mathbf{y}}} + \underbrace{\mathbf{v}_t^T Q_{\mathbf{v}} \mathbf{v}_t}_{J_{\mathbf{y}}} \right] + \underbrace{q_z \mathbf{z}^T}_{J_z}$$

$$(36)$$

For, $t \in T$ s.t. (7) - (10), (12) –(21), and (25) - (35). Where.

- $u_t = [u_1(t), u_2(t)]^T$ represents the acceleration/deceleration instructions to the two s-CAVs at control sample step t;
- $w_t = [\Delta v_1(t), \Delta v_2(t)]^T$ and $\Delta v_i(t)$ represents speed deviations of s-CAVs (i = 1 or 2) from the maximum speed \bar{v} ;
- y_t and η_t respectively denote the flow propagation defined by (29) at time step t and the car-following relationship defined by (3).
- *a* represents the relative speed of two s-CAVs.
- $x = [\Delta x(t) = x_1(t) x_2(t) \tilde{d}]_{t=1}^T$ represents the deviations of the spacing between the two subject CAVs from the pre-defined desired spacing \tilde{d} during the prediction horizon.
- Q_{ll} , Q_{ω} , Q_{φ} , Q_{η} and Q_{ω} are 2 \times 2 diagonal weight matrices and q_{ω} is weight vectors, i.e., $Q_{\omega} = \frac{1}{\left(\overline{v_{x}} v_{x}\right)^{2}} \begin{bmatrix} q_{1,\omega} & \\ & q_{2,\omega} \end{bmatrix}$, which are normalized by the maximum possible speed deviation, $q_{l,\omega}$ is a tunable weighting parameter.

The MPC involves six items in the objective function to balance the synchronization and traffic efficiency. Specifically, we evaluate traffic efficiency in this context from three perspectives: (i) the traffic smoothness, (ii) s-CAVs' speed, and (iii) upstream traffic propagation. Accordingly, the first item J_u in the objective function puts a penalty on the s-CAVs' control inputs to promote mild vehicle acceleration/deceleration so that we can keep surrounding traffic smoothness. The second item J_w seeks to sustain s-CAVs' speed so that they won't block traffic to facilitate synchronization. The third item J_y maximizes the volume of traffic propagating from the upstream to the downstream cells during the synchronization control. Therefore, the first three items J_u to J_y together help maintain a satisfying traffic efficiency during the synchronization process.

On the other hand, we factor in three aspects to ensure the synchronization efficiency: (i) positioning the s-CAV pair in the carfollowing mode, (ii) stabilizing the spacing of the two s-CAVs' to the desired value, and (iii) harmonizing the speed of the two s-CAVs. Correspondingly, J_{η} in the objective function rewards the duration that one s-CAV is following the other s-CAV. Specifically, we use summation of variable $\eta_{i,i'}^l(t)$ to model this car-following duration. $\eta_{i,i'}^l(t)$ is defined in Eq. (3) indicates whether s-CAV(i) follows s-CAV(i') at timestep t. The fifth term J_5 penalizes on the variation of the relative speed between the two s-CAVs. To be noted, J_s benefits both synchronization efficiency and traffic smoothness. And the last item J_s penalizes on the spacing deviation to push the two s-CAVs approach and then form a platoon efficiently. Table 1 summarizes the six factors and the corresponding weights.

Clearly, we should design the weight matrices/vector Q_{uv} , Q_{uv} , Q

meantime, we notice that the two s-CAVs will physically experience two dynamic traffic states below during the synchronization.

- (i) State q_1 : catch-up state, during which the two s-CAVs on different lanes seek to approach each other and form a car-following mode.
- (ii) State q_2 : platooning state, during which the two s-CAVs try to stabilize their spacing and relative speed to form a platoon on the same lane.

Under these two states, the synchronization control has different priorities for the items in the objective function. Under state q_1 , the *s*-CAVs are far apart and drive in different lanes. It is of greater importance to move these two *s*-CAVs closer to the same lane and position them in car-following mode (J_{η}) than harmonizing their speed and spacing (J_{ε} and J_{ε}). Under state q_2 in which the *s*-CAVs are already under the car-following mode, harmonizing their speed and stabilizing spacing becomes the main focus.

Considering the above problem feature and complexity, we further transfer the multi-objective MPC in (36) into a hybrid MPCs consisting of two sequential MPCs. Specifically, when the pair of *s*-CAVs is initially far away from each other (i.e., under state q_1). Accordingly, MPC-I in (37) is used to conduct the synchronization control, only including the objectives in J_u to J_η (excludes J_e and J_e) to encourage one *s*-CAV catching up the other promptly and then following it in the same lane. Under this stage, stabilizing spacing and relative speed are not our emphases.

5.1.1. MPC-I

$$Min \ \Gamma_1(u_t) = \sum_{t=0}^{T-1} \frac{1}{2} \left[\underbrace{\mathbf{u}_t^T Q_{\mathbf{u}} \mathbf{u}_t}_{J_{\mathbf{u}}} + \underbrace{\mathbf{w}_t^T Q_{\mathbf{w}} \mathbf{w}_t}_{J_{\mathbf{w}}} - \underbrace{\mathbf{y}_t^T Q_{\mathbf{y}} \mathbf{y}_t}_{J_{\mathbf{v}}} - \underbrace{\eta_t^T Q_{\eta} \eta_t}_{J_{\eta}} \right]$$

$$(37)$$

For, $t \in T$ s.t. (7) - (10), (12) - (21), and (25) - (35).

Once the following s-CAV successfully catches up the other s-CAV and they start to run in a car-following mode in the same lane, it triggers the switching signal, by which the two s-CAVs switch to the platooning state q_2 . Accordingly, the synchronization control switches to the MPC-II in (38). It focuses on maintaining the spacing of s-CAVs to the desired spacing and synchronize their speed. Accordingly, the optimizer in (38) excludes the term J_{η} in (36) with additional constraint $\sum_{l \in L} \eta_{i,l}^l(t) = 1$ to ensure s-CAVs stay in the same lane.

5.1.2. MPC-II

$$Min \ \Gamma_2(u_t) = \sum_{t=0}^{T-1} \frac{1}{2} \left[\underbrace{\mathbf{u}_t^T Q_u \mathbf{u}_t}_{J_u} + \underbrace{\mathbf{w}_t^T Q_w \mathbf{w}_t}_{J_w} - \underbrace{\mathbf{y}_t^T Q_y \mathbf{y}_t}_{J_v} + \underbrace{\mathbf{v}_t^T Q_v \mathbf{v}_t}_{J_z} \right] + \underbrace{q_z \mathbf{z}^T}_{J_z}$$

$$(38)$$

For, $t \in T$

$$\text{s.t. } \sum_{l \in L} \eta_{i,i^{'}}^{l}(t) = 1, \ \forall \ i,i^{'} \in I, t \in T$$

(7) - (10), (12) - (21), and (25) - (35).

Note that both MPC-I and MPC-II want to sustain traffic efficiency, even though they emphasize on different aspects of synchronization efficiency. Therefore, both of them involve speed fluctuation (J_u), speed deviation (J_w) and upstream traffic efficiency (J_y) in the objective functions. The feasibility of the hybrid MPC system is analyzed in Section 6.

5.2. Weighting strategies

Even though the hybrid MPC system reduces the weighting complexity in the objective function by decorrelating the items in (36) regarding the synchronization efficiency into two MPCs, each is still a multi-objective optimizer, aiming to balance the traffic and synchronization efficiency in the respective state. Moreover, we noticed that control priority may vary according to the change of the initial traffic state at each control time stamp. Taking the catch-up state (q_1) as an example, we explain this thought by the two initial states: (i) two s-CAVs drive with normal speed in two non-adjacent lanes; (ii) two s-CAVs drive with slow speed in two adjacent lanes. Recall that J_w in the objective function of MPC-I in (37) aims to sustain s-CAVs' speeds without causing adverse traffic impact, and J_{η} seeks to position s-CAVs in the car-following mode. Clearly, each state favors either J_w or J_{η} and it encourages us to use different weight schemes toward J_w and J_{η} for the best synchronization control. More exactly, we want to award J_{η} more under initial state (i) to position the two s-CAVs in the car-following mode quickly but give priority to J_w under the initial state (ii) to speed up s-CAVs and mitigate their adverse traffic impact. One the other hand, we found that only the weights of J_w and J_{η} in MPC-I and the weights of J_w and J_z in MPC-II need to be adaptively adjusted according to the initial states, while J_{tb} J_y (and J_z), respectively facilitating traffic smoothness, upstream traffic efficiency, (and s-CAV speed harmonization), should be consistently considered under any initial states when the control is in the catch-up state (q_1) (and platooning state (q_2)). Therefore, the adaptive weighting strategies will mainly focus

on the tradeoff between J_w and J_n in MPC-I (J_w and J_z in MPC-II).

To develop the weighting strategies for MPC-I, we first introduce the optimality loss regarding J_w and J_η . It should be noted that J_w in the objective function (37) penalizes s-CAVs' speed deviation from the maximum speed, $\bar{\nu}_x$. Thus, it reaches to the minimum value when the s-CAVs drive at the maximum speed. In the meantime, J_η in the objective function (37) rewards the duration that the two s-CAVs are running under the car-following mode, and it gains more values when s-CAVs drive in the same lane. Invoked by these observations, we first introduce (39) to measure the optimality loss of J_w under a given control law.

$$\Delta J_{\omega,i}(t) = \frac{\overline{v}_x t \delta - x_i(t)}{\overline{v}_\omega t \delta}, \ t \in \mathbb{Z}^+$$
(39)

where $\bar{v}_x t \delta$ represents the furthest longitudinal position that s-CAV(i) can reach up to the time step t if it drives at the maximum speed \bar{v}_x ; $x_i(t)$ is the actual position of s-CAV(i) at step t. Then, $\Delta J_{\infty,i}(t)$ represents the normalized loss of s-CAV's longitudinal displacement and it characterizes the optimality loss of the control regarding the objective in J_∞ . A smaller $\Delta J_{\infty,i}(t)$ indicates a smaller optimality loss of J_∞ and thus, a smaller weight can be put on J_∞ , and vice versa.

Following a similar idea, we use (40) to characterize the optimality loss of the reward in J_{η} under a given control law.

$$\Delta J_{\eta}(t) = \frac{|y_1(t) - y_2(t)|}{\overline{y}^L - y^L}, t \in \mathbb{Z}^+$$
(40)

where $|y_1(t) - y_2(t)|$ is the lateral spacing between the two *s*-CAVs and $\overline{y}^L - \underline{y}^L$ is the road width. Clearly, the control law gains small rewards from J_{η} in the objective funcation (i.e., ΔJ_{η} is large) when *s*-CAVs move in different lanes, but a large and accumulated reward when the two *s*-CAVs run in the same lane (i.e., $\Delta J_{\eta} = 0$).

Using the two optimality losses, we develop the weighting strategy for MPC-I in (41), which adaptively tunes the weights of J_{m} and J_{η} in (37) aiming to have the following s-CAV to quickly catch up the leading s-CAV and then follow the car-following mode in the same lane, while sustaining traffic efficiency.

$$q_{\eta} = \sum_{i \in I} \alpha_i q_{i,\sigma} \xi_{i,t}^I, \xi_{i,t}^I = \frac{\Delta J_{\eta}}{\Delta J_{\sigma,i}}$$

$$\tag{41}$$

where $q_{i,w}$ and q_{η} are the weight assigned to objective J_{w} and J_{η} , respectively. α_{l} is a tunable parameter, and $\xi_{i,t}^{l}$ is a scaling parameter equal to the ratio of the optimality loss of J_{η} to that of J_{w} . The key idea in (41) is that if the two s-CAVs are moving in different lanes (i.e., a large $\Delta J_{\eta}(t)$), we give a higher priority to J_{η} in (37) through varying the scaling parameter $\xi_{i,t}^{l}$ to encourage lane changes which moves two s-CAVs in the same lane and position them in a car-following mode unless they drive too low (i.e., a large $\Delta J_{w,i}(t)$), i.e., weigh J_{η} over J_{w} in the objective function, and vice versa.

To develop the weighting strategy for MPC-II, we notice that the last item J_s in the objective function (38) focus on stabilizing the spacing between two s-CAVs (i.e., penalizing the deviation of s-CAVs' spacing from the desired spacing). Following the same idea as before, we introduce (42) to measure the optimality loss regarding the objective J_s under a given control law.

$$\Delta J_{\varepsilon}(t) = \frac{|x_2(t) - x_1(t) - \widetilde{d}|}{\widetilde{d}}$$
(42)

where $|x_2(t) - x_1(t) - \tilde{d}|$ is the deviation of s-CAVs' spacing from the desired spacing, \tilde{d} . Then, $\Delta J_x(t)$ represents the normalized spacing deviation of s-CAVs and it characterizes the optimality loss of the control regarding the objective J_x . A larger $\Delta J_x(t)$ indicates a larger optimality loss of J_x (larger deviation from desired spacing) and thus, J_x can be prioritized, and vice versa.

Using the two optimality losses $\Delta J_{w,i}$ in (39) and ΔJ_z in (42), we develop the adaptive weighting strategy for MPC-II in (43), aiming to keep the two *s*-CAVs in an efficient platooning mode, while sustaining the traffic efficiency.

$$q_{z} = \sum_{i \in I} \alpha_{i} q_{i,\omega} \xi_{i,t}^{II}, \ \xi_{i,t}^{II} = \frac{\Delta J_{z}}{\Delta J_{\omega,i}}$$

$$(43)$$

where $q_{i,w}$ and q_x are the weights assigned to objective J_w and J_x , respectively. α_i is a tunable parameter and $\xi_{i,t}^{II}$ is a scaling parameter equal to the ratio of the optimality loss of J_x to that of J_w . Here, the main idea is that if the spacing of the two s-CAVs deviates too much from the desired spacing (a large ΔJ_x), we give a high priority to J_x in the objective function (38) through the scaling parameter $\xi_{i,t}^{II}$, which encourages s-CAVs to adjust their speed and achieve the desired spacing unless they drive too slow and block the traffic (a large $\Delta J_{w,i}$), and vice versa.

We also notice that $\Delta J_{w,i}=0$ is a feasible scenario for both MPC-I and II, and it will raise the numerical issues to apply (42) and (43). To address this problem, we limit the scaling parameters $\xi_{i,t}^I$ (and $\xi_{i,t}^{II}$) to a numerical range, i.e., $\xi_{i,t}^I \in [0,\xi_{max}^I]$, where ξ_{max}^I is a given parameter to bound $\xi_{i,t}^I$ and avoid numerical issue. In addition, the scaling parameter $\xi_{i,t}^I$ (and $\xi_{i,t}^{II}$) will be calculated at each sample time point t and keep constant within a prediction horizon.

6. Recursive feasibility of the constraint set

As the MPC is implemented recursively at each time step, a fundamental question is whether the MPC can find a feasible control law at each time step t (i.e., whether the constraint set of the MPC optimizer is non-empty at each time step t), given the platoon system starts from an initial feasible condition. A system is called recursive (persistent) feasible (Mayne, 2014) if the answer to this question is affirmative. Apparently, it is extremely important for the applicability of the MPC in practical implementation. Therefore, this section will investigate the recursive feasibility of the MPC-I (37) and MPC-II (38). Before that, we need to clarify two points. Recall the MPC will reset the initial condition at each control time step by recognizing new neighbor vehicles Ω , their positions and velocities. Therefore, the MPC accounts for the uncertainty and dynamics of neighbor traffic and surrounding vehicles. A new control law at each step can correct control errors resulting from previous steps due to inaccurate predictions. Moreover, given MPC-I and MPC-II only involve two s-CAVs and a limited number of neighbor vehicles, their model sizes are relatively small and can be efficiently solved by a commercial solver, i.e., Gurobi, within the control interval. Therefore, the control continuity is sustained. These views are fundamentals and prerequisites of the recursive feasibility analysis.

Given MPC-I and MPC-II share the same constraint set, we will only prove that the recursive feasibility of MPC-I. To do that, we first formally define this constraint set $\mathcal{P}(u(t), \chi(t))$ by (44), and want to prove that if $\mathcal{P}(u(t-1), \chi(t-1))$ is nonempty at control step t-1, then the constraint set $\mathcal{P}(u(t), \beta(t))$ is nonempty at control step t, $t \in \mathbb{Z}_+$.

$$\mathscr{P}(u(t),\chi(t)) = \left\{ u(t) \in \mathbb{R}^{T|I|}, \chi(t) \in \mathbb{B}^{m} | g_t(u(t),\chi(t)) \le 0 \right\}, \forall t \in \mathbb{Z}_+$$

$$\tag{44}$$

where $\mathbb{B} = \{0,1\}$, and $g_t(u(t),\chi(t)) \le 0$ is the constraint set defined by constraints (7) - (10), (12) - (21), and (26) - (35). $\chi(t)$ is the set of binary variables, respectively including vehicles' lane memberships, relative positions of vehicle pairs and cell memberships, i.e., $\chi(t) = \{\gamma(t), \rho(t), \eta(t), \phi(t)\}$.

The standard approach to prove the recursive feasibility of an MPC is to show there exists a control-invariant set that contains the origin. However, it is generally difficult to prove the recursive feasibility of an MPC with binary variables using the standard approach. This is because the combinations of binary variables lead to an enormous number of solution spaces, and it is hard to show the existence of a control-invariant set among them (Marcucci and Tedrake, 2020). However, the constraint set $\mathcal{P}(u(t),\chi(t))$ in this study presents unique features as follows which can facilitate our proof. (i) The values of binary variables in $\chi(t)$ are determined by the leading (following) relationships of the two s-CAVs and their neighbor vehicles, which presents a limited number of cases (will define them in detail in the proof later). Accordingly, the constraint set (44) can be divided into small constraint sets that only contain the continuous variables u(t). (ii) Constraints (28) - (35), which describe the upstream traffic propagation, are naturally feasible once vehicles' cell membership, i.e., binary variables $\phi(t)$, are determined. Thus, we only consider constraints (7) - (10), (12) - (21), (26), and (27), and omit constraints (28) - (35) in our proof. Taking advantage of these features, we prove the recursive feasibility of MPC-I in Theorem 1.

Mainly, Theorem 1 claims that MPC-I is feasible at step t, i.e., $\mathscr{P}(u(t), \beta(t)) \neq \emptyset$ if the four conditions are satisfied. Specifically, Condition (i) calls for the feasibility of MPC-I at step t-1, i.e., $\mathscr{P}(u(t-1), \chi(t-1)) \neq \emptyset$. Condition (ii) requires that neighbor vehicles follow the speed limits as the subject CAVs, i.e., $\widehat{v}_{\omega}(t) \in [\underline{v}_x, \overline{v}_x]$, $\forall \omega \in \Omega_h \cup \Omega_c$. This is a reasonable condition since in a normal traffic, every vehicle on the road follows the regulatory speed limits. Condition (iii) requires the reaction time of neighbor HDVs to satisfy $\tau_{\omega} \leq \overline{\tau}_{\omega}$, $\forall \omega \in \Omega_h$. We will demonstrate the rationality of the bound in the remark followed by our proof of Theorem 1. Condition (iv) requires that when an n-CAV(ω) follows a s-CAV(i), the relative speed between them satisfies $v_i(t) - \widehat{v}_{\omega}(t) \geq \frac{\widetilde{a}_i(t-1)\delta(B-\frac{1}{2})}{A}$, $\forall \omega \in \Omega_c$. In other words, the speed of s-CAV, $v_i(t)$, $\forall i \in I$, is bounded by $v_i(t) \geq \widehat{v}_{\omega}(t) + \frac{\widetilde{a}_i(t-1)\delta(B-\frac{1}{2})}{A}$. We will show that this condition is recursively satisfied if it holds at the beginning of the prediction horizon, i.e., t=0, in Theorem 1. Moreover, by plugging in the values of parameters (Xiao et al., 2017), i.e., $\delta=1$ s, A=0.1836, B=0.8163, $\widetilde{a}_i(t-1) = \underline{a}_x = -6$ m/s^2 , we can obtain that $\frac{\widetilde{a}_i(t-1)\delta(B-\frac{1}{2})}{A} = -10.33$ m/s (or -23.11mph). It indicates that Condition (iv) is satisfied in most of the normal traffic scenarios.

Theorem 1. $\mathscr{P}(u(t), \chi(t))$ is recursively feasible, i.e., $\mathscr{P}(u(t), \chi(t)) \neq \emptyset$, $\forall t \in \mathbb{Z}_+$, if the following conditions hold.

```
\begin{split} &\text{(i). } \mathscr{P}(\pmb{u}(t-1), \pmb{\chi}(t-1)) \neq \varnothing, \, \forall t \in \mathbb{Z}_+. \\ &\text{(ii). } \underline{\nu_{\mathbf{x}}} \leq \widehat{\nu}_{\omega}(t) \leq \overline{\nu_{\mathbf{x}}}, \, \forall t \in \mathbb{Z}_+, \omega \in \Omega_h \cup \Omega_{\mathbf{c}}. \\ &\text{(iii). } \tau_{\omega} \leq \overline{\tau}_{\omega}, \, \forall \omega \in \Omega_h, \, \text{where } \overline{\tau}_{\omega} = \frac{-(\nu_{\mathbf{x}} - 5a_{\mathbf{x}}) - \sqrt{\left(\nu_{\mathbf{x}} - 5a_{\mathbf{x}}\right)^2 - 24a_{\mathbf{x}}d_{\omega}}}{2a_{\mathbf{x}}}, \, \omega \in \Omega_h \end{split}
```

(iv). The speeds of n-CAVs(ω) and its leading vehicle, i, satisfy $v_i(t) - \widehat{v}_{\omega}(t) \ge \frac{\widetilde{a}_i(t-1)\delta\left(B-\frac{1}{2}\right)}{A}$, where $\widetilde{a}_i(t) = \max\left[\underline{a_x}, \underline{a_{i,v}}(t)\right]$ and $\underline{a_{i,v}}(t) = \frac{v_x - v_x^x(t)}{\delta}$.

Proof. To begin with, we have two s-CAVs in the study and we noticed that except for the safety constraint (12), in which two s-CAVs are coupled (will discuss later in detail), the constraints in $\mathcal{P}(u(t), \chi(t))$ are formulated for each s-CAV separately. Thus, we can separate the constraint set such that $\mathcal{P}(u(t), \chi(t)) = \{\mathcal{P}(u_1(t), \chi(t)), \mathcal{P}(u_2(t), \chi(t))\}$, where $u_1(t)$ and $u_2(t)$ are respectively the control inputs for s-CAV(1) and s-CAV(2). Without loss of generality, our proof below will first focus on one s-CAV such as s-CAV(1) and then the results can be easily extended to the other s-CAV so that we can conclude Theorem 1.

To conduct the proof, we further rewrite the constraint sets $\mathcal{P}(u_1(t), \chi(t))$ in (45) according to the binary variables within the constraints.

$$\mathscr{P}(u_1(t),\chi(t)) = \mathscr{P}_u(u_1(t)) \cap \mathscr{P}_{\gamma}(u_1(t),\chi(t)) \tag{45}$$

Where,

- (1) $\mathscr{P}_u(u_1(t))$: The constraint set only includes continuous variables in Eq. (7) (10) and Eq. (17) (19) for capturing vehicle dynamics of s-CAV(1) at step $t \in T$.
- (2) $\mathscr{P}_{\chi}(u_1(t),\chi(t))$: The constraints set includes both binary variables $\chi(t)$ and continuous variables in constraints (12), (13), (15), (16), (20), (21), (26) and (27) for capturing the following relationship and safety constraints of *s*-CAV(1) at step $t \in T$.

Next, we discuss the three cases for specifying the following relationships between s-CAV(1) and its leading or following neighbor vehicles, each of which determines a set of values of the binary variables in $\chi(t)$. Case (1) considers that s-CAV(1) follows another vehicle j in lane $l^* \in L$, which can be the other s-CAV, or a n-CAV, or an HDV. A vehicle pair in this case is denoted as $1 \to j$, $\forall j \in J$. According to Eqs. (1)–(6), Case (1) determines the values of the lane membership indicators (γ) and the following relationship indicators (γ) and γ). We use $\chi_1(u_1(t))$ to denote this set of solutions shown in Eq. (46). Then, the constraints set $\mathscr{P}_{\chi}(u(t),\chi(t))$ is simplified into the constraints associated with the vehicle pair $1 \to j$, which we denote as $\mathscr{P}_{\chi}(u_1(t)|\chi_1)$.

$$\chi_{1}(u_{1}(t)) = \left\{ \gamma_{1}^{l'}(t) = 1, \gamma_{j}^{l'}(t) = 1, \eta_{1,j}^{l'}(t) = 1, \rho_{1,j}^{l'}(t) = 1, \rho_{1,j}^{l'}(t) = 1 \right\} \cup \left\{ \gamma_{1}^{l}(t) = 0, \gamma_{1}^{l}(t) = 0, \eta_{1,j}^{l}(t) = 0, \rho_{1,j}^{l}(t) = 0 \right\}_{l \in I \setminus I^{*}}, \forall j \in J, l^{*} \in L$$

$$(46)$$

For Case (2), we consider that s-CAV(1) is followed by an HDV(ω) in lane $l^* \in L$. We denote this vehicle pair as $\omega \to 1$, $\forall \omega \in \Omega_h$. Following the similar discussion used in Case (1), we determine the values of binary variables as shown in (47) according to Eqs. (1)–(6), and then simplify the constraints set $\mathscr{P}_{\chi}(u(t),\chi(t))$ to $\mathscr{P}_{\chi}(u_1(t)|\chi_2)$.

$$\chi_{2}(u_{1}(t)) = \left\{ \gamma_{\omega}^{l}(t) = 1, \gamma_{1}^{l}(t) = 1, \eta_{\omega,1}^{l}(t) = 1, \rho_{\omega,1}^{l}(t) = 1 \right\} \cup \left\{ \gamma_{1}^{l}(t) = 0, \gamma_{\omega}^{l}(t) = 0, \eta_{1,\omega}^{l}(t) = 0, \rho_{1,\omega}^{l}(t) = 0 \right\}_{l \in L \setminus l^{*}}, \forall \ \omega \in \Omega_{h}, l^{*} \in L$$

$$(47)$$

Similarly, in Case (3), we consider that s-CAV(1) is followed by a n-CAV(ω) in lane $l^* \in L$ and denote this vehicle pair as $\omega \to 1$, $\forall \omega \in \Omega_c$. Then, the binary variables' values in shown (48) can be determined by Eqs. (1)–(6). We denote $\mathscr{P}_{\chi}(u_1(t)|\chi_3)$ as the activated constraints associated with these binary variables in \mathscr{P}_2 .

$$\chi_{3}(u_{1}(t)) = \left\{ \gamma_{\omega}^{l}(t) = 1, \gamma_{1}^{l}(t) = 1, \eta_{\omega,1}^{l}(t) = 1, \rho_{\omega,1}^{l}(t) = 1, \rho_{\omega,1}^{l}(t) = 1 \right\} \cup \left\{ \gamma_{1}^{l}(t) = 0, \gamma_{\omega}^{l}(t) = 0, \eta_{1,\omega}^{l}(t) = 0, \rho_{1,\omega}^{l}(t) = 0 \right\}_{l \in I \setminus P}, \forall \omega \in \Omega_{c}, l^{*} \in L \quad (48)$$

The three cases specify the leading and following relationship of s-CAV(1) and its neighbors at any time step t. Specifically, it will always drive under Case (1) combined with either Case (2) or Case (3). Then, we reformulate the constraint set \mathcal{P}_{χ} for s-CAV(1) in (49). For example, if s-CAV(1) follows a n-CAV, and is followed by an HDV, then \mathcal{P}_{χ} is specified as $\mathcal{P}_{\chi}(u_1(t)|\chi_1) \cup \mathcal{P}_{\chi}(u_1(t)|\chi_2)$.

$$\mathcal{P}_{\chi}(u_{1}(t),\chi(t)) = \mathcal{P}_{\chi}(u_{1}(t)|\chi_{1}) \cup \mathcal{P}_{\chi}(u_{1}(t)|\chi_{2}) \cup \mathcal{P}_{\chi}(u_{1}(t)|\chi_{3}) \tag{49}$$

Built upon (49), we want to show $\mathscr{P}_u(u_1(t))\cap \mathscr{P}_\chi(u_1(t)|\chi_1)=\mathbb{U}\neq\emptyset$, and then demonstrate $\mathbb{U}\cap\mathscr{P}_\chi(u_1(t)|\chi_2)\neq\emptyset$ and $\mathbb{U}\cap\mathscr{P}_\chi(u_1(t)|\chi_3)\neq\emptyset$, given the four conditions in Theorem 1 are satisfied. This proof can be extended to $s-\mathrm{CAV}(2)$ so that we can draw the conclusion and complete the proof for Theorem 1. Below are the derivation details for each step.

Scenario I: without loss of generality, we start with the scenario that s-CAV(1) follows an HDV(ω) in a lane $l^* \in L$ (Case(1)). By plugging the values of the integer variables given in (46) into Constraints (12), (13), (15), (16), (20), (21), (26), and (27), we obtain the only activated constraint (13) in $\mathcal{P}_{\gamma}(u_1(t)|\chi_1)$, for which we introduce a new notation $\widehat{\mathcal{P}}_{1,\omega}(u_1(t))$ as follows.

$$\widehat{\gamma}_{1,\omega}(u_1(t)) := \widehat{x}_{\varpi}(t) - x_1(t) - \left(L_1 + \tau_1 v_1^x(t) - \frac{\left[v_1^x(t) - \underline{v_x}\right]^2}{2a_x}\right), \forall \ \omega \in \Omega_h$$
(50)

Then, combining constraints (17) and (18) in $\mathscr{P}_u(u_1(t))$, we ensure that the speed of HDV(ω) follows $\underline{v_x} \leq \widehat{v_\omega}(t) \leq \overline{v_x}$, which confirms Condition (ii) in Theorem 1. Now, $\mathscr{P}_u(u_1(t)) \cap \mathscr{P}_\chi(u_1(t)|\chi_1) = \mathbb{U}(u_1(t))$ is the joint constraint set involving constraints (7)–(10) and safety constraint (50). We claim that $\mathbb{U}(u_1(t))$ is non-empty and given in (51) for any $\widehat{v}_\omega(t) \in [\underline{v_x}, \overline{v_x}]$ by referring to the Lemma 4.1 in (Gong et al., 2016) without providing the detailed proof.

$$u_1(t) \in \mathbb{U}(u_1(t)) = \left[\max \left\{ \underline{a_x}, \underline{a_{1,\nu}}(t) \right\}, \min \left\{ \overline{a_x}, \overline{a_{1,\nu}}(t), \overline{a_{1,d}}(t) \right\} \right]$$

$$(51)$$

Where

$$\frac{a_{1,\nu}}{\delta}(t) = \frac{v_x - v_1^x(t)}{\delta} \le 0 \tag{51.1}$$

$$\overline{a_{1,v}}(t) = \frac{\overline{v_x} - v_1^v(t)}{\delta} \ge 0 \tag{51.2}$$

$$\overline{a_{1,d}}(t) = \frac{3}{2} \underline{a_x} + \underline{a_{1,v}} - \frac{a_x}{\delta^2} \sqrt{B(t)}$$
 (51.3)

$$B(t) = \frac{\left(v_1^{\mathsf{x}}(t-1) - \underline{v_x}\right)^2 \delta^2}{a_x^2} + \frac{\delta^3 \left(v_1^{\mathsf{x}}(t-1) - \underline{v_x}\right)}{-a_x} + \frac{9}{4} \delta^4 + \left(\frac{2\delta^2}{-a_x}\right) \left[\left(\frac{\widehat{v}_{\omega}(t-1) + \widehat{v}_{\omega}(t)}{2} - \underline{v_x}\right) \delta + \widehat{\rho}_{1,\omega}(u_1(t-1))\right] \ge 0 \tag{51.4}$$

Built upon $\mathbb{U}(u_1(t))$, we next consider that this s-CAV(1) is followed by an HDV(ω), $\forall \omega \in \Omega_h$ (i.e., a scenario formed by Case (1) combined with Case (2)). By plugging the values of the binary variables given in (47) into constraints (12), (13), (15), (16), (20), (21), (26), and (27), we find that the only activated constraints in $\mathcal{P}_\chi(u_1(t)|\chi_2)$ are Eqs. (15) and (16), which determines the spacing of the HDV. Therefore, the activated constraints in $\mathcal{P}_\chi(u_1(t)|\chi_2)$ are given in the set of (52), where $k = \frac{\tau_\omega}{\delta} \in \mathbb{Z}_+$. Clearly, (52) will not be empty as long as there exists spacings $s_{\omega,1} \geq 0$. Note that k is the number of time steps corresponding to the HDV's response delay to its leading vehicle. When $k \leq 1$ for which the HDV can quickly respond to the control of s-CAV(1), we only need to show that there exists a positive spacing $s_{\omega,1}$ at step t+1 in (52). When k>1, for which there exists a response delay of HDV that is greater than the step size, we have to examine the constraints in extra time steps, t+k and afterwards. Without loss of generality, we assume k>1, given that the feasibility can be easily shown for $k \leq 1$ if the feasibility holds for k>1.

$$v_1(t+k) = v_1(t) + \delta k u_1(t) \tag{52.1}$$

$$x_1(t+k) = x_1(t) + \delta k v_1(t) + \frac{(\delta k)^2}{2} u_1(t)$$
(52.2)

$$\widehat{v}_{\omega}(t+k) = \max\left\{\underline{v}_{x}, \frac{\delta}{\tau_{\omega}}\left(s_{\omega,1}(t) - d_{\omega}\right)\right\}$$
(52.3)

$$\widehat{v}_{\omega}(t+k) = \min\left\{\overline{v_{x}}, \frac{\delta}{\tau_{\omega}}\left(s_{\omega,1}(t) - d_{\omega}\right)\right\}$$
 (52.4)

$$\widehat{x}_{\omega}(t+k) = \widehat{x}_{\omega}(t) + \tau_{\omega}\widehat{v}_{\omega}(t)$$
 (52.5)

$$s_{\omega,1}(t+k) = x_1(t+k) - \hat{x}_{\omega}(t+k)$$
 (52.6)

As a result, we seek to prove that there exists $u_1(t) \in \mathbb{U}(u_1(t))$ such that the spacing $s_{\omega,1} \geq 0$ in step t+k and afterward. Given $\mathscr{P}_{\chi}(u_1(t-1)|\chi_2)$ is feasible, we have $s_{\omega,1}(t-1) \geq 0$. Then we discuss it in two situations as follows.

- (i) When $0 \le s_{\omega,1}(t-1) < \underline{\nu_x} \frac{\tau_\omega}{\delta} + d_\omega$, according to Eq. (52.4), we have $\widehat{\nu}_\omega(t-1+k) = \underline{\nu_x}$. Given $\widehat{\nu}_\omega(t-1+k) = \underline{\nu_x} \le \nu_1(t-1+k)$, we can expect that $s_{\omega,1}(t-1+k) > s_{\omega,1}(t-1) \ge 0$.

 (ii) When $s_{\omega,1}(t-1) \ge \underline{\nu_x} \frac{\tau_\omega}{\delta} + d_\omega$, we further consider two more subcases: (1) $\underline{\nu_x} \frac{\tau_\omega}{\delta} + d_\omega \le s_{\omega,1}(t-1) < \overline{\nu_x} \frac{\tau_\omega}{\delta} + d_\omega$. It is equivalent to
- (ii) When $s_{\omega,1}(t-1) \geq \underline{\nu_x} \frac{\tau_\omega}{\delta} + d_\omega$, we further consider two more subcases: (1) $\underline{\nu_x} \frac{\tau_\omega}{\delta} + d_\omega \leq s_{\omega,1}(t-1) < \overline{\nu_x} \frac{\tau_\omega}{\delta} + d_\omega$. It is equivalent to $\underline{\nu_x} \leq \frac{\delta}{\tau_\omega} (s_{\omega,1}(t-1) d_\omega) \leq \overline{\nu_x}$. Based on (52.3), we have $\widehat{\nu}_\omega(t-1+k) = \max\left\{\underline{\nu_x}, \frac{\delta}{\tau_\omega} (s_{\omega,1}(t-1) d_\omega)\right\} = \frac{\delta}{\tau_\omega} (s_{\omega,1}(t-1) d_\omega)$, which further indicates $s_{\omega,1}(t-1) = \widehat{\nu}_\omega(t-1+k) \frac{\tau_\omega}{\delta} + d_\omega$. Then, we consider the other subcase (2) when $s_{\omega,1}(t-1) \geq \overline{\nu_x} \frac{\tau_\omega}{\delta} + d_\omega$. It means $\overline{\nu_x} \leq \frac{\delta}{\tau_\omega} (s_{\omega,1}(t-1) d_\omega)$. According to (52.4), $\widehat{\nu}_\omega(t-1+k) = \min\left\{\overline{\nu_x}, \frac{\delta}{\tau_\omega} (s_{\omega,1}(t-1) d_\omega)\right\} = \overline{\nu_x}$. Therefore, we have $s_{\omega,1}(t-1) \geq \widehat{\nu}_\omega(t-1+k) \frac{\tau_\omega}{\delta} + d_\omega$. Combining the results from the two subcases, we conclude that $s_{\omega,1}(t-1)$ satisfy $s_{\omega,1}(t-1) \geq \widehat{\nu}_\omega(t-1+k) \frac{\tau_\omega}{\delta} + d_\omega$.

Now, based on (52.1) - (52.6), we rewrite the spacing $s_{\omega,i}$ in a recursive form as follows.

$$s_{\omega,1}(t+nk) = s_{\omega,1}(t+(n-1)k) - s_{\omega,1}(t+(n-2)k) + \frac{1}{2}u_1(t+(n-1)k)\delta^2 + v_1(t+(n-1)k)\delta + d_{\omega}, \ \forall n \in \mathbb{Z}_+$$
 (53)

According to (52.1), when $u_1(t)$ takes the minimum value, $v_1(t+k)$ reaches the minimum value. Then, upon (53), we have $s_{\omega,1}(t+nk)$ reach the minimum value if $u_1(t+n'k)$ takes the minimum value for $\forall n'=0,1,2...,n$. Therefore, in order to show that $s_{\omega,1}(t+nk) > 0, \forall n \in \mathbb{Z}_+$, we consider an extreme scenario where $u_1(t+n'k)$ takes the minimum value (i.e., the maximum deceleration) defined by $\mathbb{U}, \forall n'=0,1,2...,n$. From (51), the potential maximum deceleration in \mathbb{U} is \underline{a}_x and the corresponding smallest spacing defined in (53) is

given by $s_{\omega,1}(t+5k) = \widehat{v}_{\omega}(t-1+k)\tau_{\omega} + d_{\omega} + 6\underline{a_x}\tau_{\omega}^2$ (see Appendix B for the derivation details). Given that $\tau_{\omega} \leq \frac{-(\underline{v_x}-5\underline{a_x})-\sqrt{(\underline{v_x}-5\underline{a_x})^2-24\underline{a_x}d_{\omega}}}{2\underline{a_x}}$ from Condition (iii) of Theorem 1, we have $s_{\omega,1}(t+5k) \geq 0$, which confirms that the spacing $s_{\omega,1}(t+nk)$ will be positive for any input $u_1(t) \in \mathbb{U}$, if Condition (iii) holds.

Here we want to consider a state transition and its feasibility further. Namely, s-CAV(2) cuts in between s-CAV(1) and its follower, HDV(ω) at step t. Then, the scenario transfers to the special one where s-CAV(2) follows s-CAV(1) and is followed by the HDV(ω). This transition makes the constraint of the two s-CAVs correlated in the safety constraint. Then, we need to prove the recursive feasibility regarding s-CAV(2) in this special scenario. Mainly, we want to show $\mathcal{P}_u(u_2(t)) \cap \mathcal{P}_\chi(u_2(t)|\chi_1) = \mathbb{U}(u_2(t)) \neq \emptyset$, and then there exists $u_2(t) \in \mathbb{U}(u_2(t))$ such that $\mathcal{P}_u(u_2(t)) \cap \mathcal{P}_\chi(u_2(t)|\chi_2) \neq \emptyset$, given Conditions (i)-(iv) in Theorem 1 hold. The proof is similar to the argument above, thus we only present the main idea as follows. First of all, with the given following relationship, we can specify the relevant integer variables in(46), i.e., $\gamma_1^r(t) = 1, \gamma_2^r(t) = 1, \eta_{2,1}^r(t) = 1, \rho_{2,1}^r(t) = 1$, and then the only activated constraint in $\mathcal{P}_\chi(u_2(t)|\chi_1)$

is constraint (12), which couples two s-CAVs. According to constraint (10), $v_2(t) \in [v_x, \overline{v_x}]$, we confirm Condition (ii) of Theorem 1. Then, following the same argument for s-CAV(1) under Case (1), we can also show that $\mathbb{U}(u_2(t)) \neq \emptyset$. Next, given the cutting-in occurs at time step t, we have $\eta^p_{\omega,2}(t)=1$ and $\eta^p_{\omega,2}(t-1)=0$ (i.e., HDV(ω) starts to follow s-CAV(2) at step t but not t-1). Accordingly, the safety constraint (20) is "turned on" to ensure the spacing between s-CAV(2) and the HDV ω satisfying $s_{\omega,2}(t) = x_2(t) - \widehat{x}_{\omega}(t) \geq \frac{\tau_{\omega}}{s}\widehat{V}_{\omega}(t)$ $+d_{\omega}$. Then, through the similar discussion for s-CAV(1) under the scenario of Case (1) combined with Case (2), we can prove that $s_{\omega,2}(t)$ + nk) ≥ 0 for any control input $u_2(t) \in \mathbb{U}(u_2(t))$. The above arguments together conclude the feasibility after this state transition under Scenario I.

Scenario II is the combination of Case (1) and Case (3). Namely, we consider s-CAV(1) follow a neighbor vehicle $j \in J$ and it is followed by a n-CAV(ω) in lane $l^* \in L$. We want to show that there exists $u_1(t) \in \mathbb{U}(u_1(t))$ such that $\mathcal{P}_u(u_1(t)) \cap \mathcal{P}_\chi(u_1(t)|\chi_3) \neq \emptyset$, given that $\mathcal{P}(u_1(t-1),\chi)$ and other conditions in Theorem 1 hold. As n-CAV(ω) follows the s-CAV(1) at step t-1, we have $\eta_{t-1}^{\ell}(t-1)=1$. Accordingly, Constraint (27) is relaxed. Then the only activated constraint in $\mathcal{P}_{\chi}(u_1(t)|\chi_3)$ is Eq. (26). Given that the CACC scheme is operated with $k_1 = 0.01s^{-2}$, $k_2 = 1.6 s^{-1}$ and $t_d = 0.6s$ (Xiao et al., 2017). Accordingly, we have $k_2 \gg k_1$, A = 0.1836 and B = 0.8163, and $C \approx 0$ from the formulations of A and B in (25). Therefore, we can drop the items related with C in Eq. (26), and then it becomes the following Eq. (54.1). Now, the activated constraints in $\mathcal{P}_u(u_1(t)) \cap \mathcal{P}_\chi(u_1(t)|\chi_3)$ are presented in Eqs. (54.1)–(54.5).

$$\widehat{v}_{\omega}(t+1) = A\widehat{v}_{\omega}(t) + Bv_1(t+1) \tag{54.1}$$

$$\widehat{x}_{\omega}(t+1) = \widehat{x}_{\omega}(t) + \delta\widehat{v}_{\omega}(t+1) \tag{54.2}$$

$$v_1(t+1) = v_1(t) + \delta u_1(t) \tag{54.3}$$

$$x_1(t+1) = x_1(t) + \delta v_1(t) + \frac{\delta^2}{2} u_1(t)$$
(54.4)

$$s_{\omega,1}(t) = x_1(t) - \hat{x}_{\omega}(t)$$
 (54.5)

Clearly, to prove $\mathscr{P}_u(u_1(t)) \cap \mathscr{P}_\chi(u_1(t)|\chi_3) \neq \emptyset$, we want to show there exists $u_1(t-1) \in \mathbb{U}(u_1(t-1))$ such that the spacing at step tsatisfies $s_{\omega,1}(t) \geq 0$. Our poof below first demonstrates that if Condition (iv): $v_1(t-1) - \widehat{v}_{\omega}(t-1) \geq \frac{\widetilde{a}_1(t-1)\delta\left(B-\frac{1}{2}\right)}{a}$ in Theorem 1 holds at step t-1, then it does at step t also, i.e., $\nu_1(t)-\widehat{\nu}_{\omega}(t)\geq \frac{\widetilde{\alpha}_1(t-1)\delta(B-\frac{1}{2})}{A}$.

To begin with, we write the relative speed, $\nu_1(t)-\widehat{\nu}_{\omega}(t)$ between n-CAV (ω) and s-CAV(1) in (55.1) derived from (54.1) and (54.3).

$$v_1(t) - \hat{v}_{\omega}(t) = v_1(t) - A\hat{v}_{\omega}(t-1) - Bv_1(t) = A[v_1(t-1) - \hat{v}_{\omega}(t-1)] + A\delta u_1(t-1)$$
(55.1)

Clearly, $v_1(t-1) - \hat{v}_{\omega}(t-1)$ in (55.1) is bounded according to Condition (iv). We next discuss the lower bounds of the $u_1(t-1)$ in (55.1). To do that, we define a deceleration lower bound $\widehat{\underline{a}}_1(t-1) = \frac{B(B-\frac{1}{2})\widehat{\alpha}_1(t-1)}{A^2}$. Given A=0.1836 and B=0.8163, we have $\widehat{\underline{a}}_1(t-1)$ $=7.66\ \widetilde{a}_1(t-1)\leq \widetilde{a}_1(t-1)\leq 0.\ \text{Then, given }\widetilde{a}_1(t-1)=\max\Big[\underline{a}_{\underline{x}},\underline{a}_{\underline{i},\underline{v}}(t-1)\Big]\ \text{in Condition (iv), we have }\underline{\widehat{a}}_1(t-1)\leq \max\Big[\underline{a}_{\underline{x}},\underline{a}_{\underline{i},\underline{v}}(t-1)\Big].$ Recall that $\mathbb{U} = \left[\max\left\{\underline{a_x}, a_{1,\nu}(t)\right\}, \min\left\{\overline{a_x}, \overline{a_{1,\nu}}(t), \overline{a_{1,d}}(t)\right\}\right]$ given in (51), we can find a $u_1(t-1) \in \mathbb{U}$, so that $u_1(t-1) \geq \underline{\widehat{a}}_1(t-1)$. Then, we can further process (55.1) as follows.

$$v_{1}(t) - \widehat{v}_{\omega}(t) = A[v_{1}(t-1) - \widehat{v}_{\omega}(t-1)] + A\delta u_{1}(t-1) \ge -\widetilde{a}_{1}(t-1)\left(\frac{1}{2} - B\right)\delta + A\delta u_{1}(t-1)$$

$$\ge \widetilde{a}_{1}(t-1)\delta\left(B - \frac{1}{2}\right) + \frac{B(B - \frac{1}{2})\widetilde{a}_{1}(t-1)\delta}{A} = \frac{\widetilde{a}_{1}(t-1)\delta(B - \frac{1}{2})}{A}$$
(55.2)

Built upon Condition (iv), we want to prove that there exists a control input $u_1(t-1) \in U(u_1(t-1))$ such that $s_{\omega,1}(t) \geq 0$. To show this result, we rewrite the spacing $s_{\omega,1}(t)$ in a recursive form in (56) based on (54.1) - (54.5).

$$s_{\omega,1}(t) = s_{\omega,1}(t-1) + A\delta[v_i(t-1) - \widehat{v}_{\omega}(t-1)] + \left(\frac{1}{2} - B\right)\delta^2 u_1(t-1)$$
(56)

Because $\mathscr{P}(u_1(t-1),\chi)$ is feasible, $s_{\omega,1}(t-1) \geq 0$. Then $s_{\omega,1}(t) \geq A\delta[\nu_1(t-1) - \widehat{\nu}_{\omega}(t-1)] + \left(\frac{1}{2} - B\right)\delta^2u_1(t-1)$. According to (51), $\mathbb{U}(u_1(t-1)) = \left\lceil \max\left\{\underline{a_x}, a_{1,\nu}(t-1)\right\}, \min\left\{\overline{a_x}, \overline{a_{1,\nu}}(t-1), \overline{a_{1,d}}(t-1)\right\} \right\rceil. \text{ Therefore, we have } u_1(t-1) \geq \max\left\{\underline{a_x}, a_{1,\nu}(t-1)\right\} = \widetilde{a}_1(t-1).$ Combining with the results in (55.2), we have $s_{\omega,1}(t) \geq A\delta[\nu_1(t-1) - \widehat{\nu}_{\omega}(t-1)] + \left(\frac{1}{2} - B\right)\delta^2u_1(t-1) \geq \widetilde{a}_1(t-1)\delta^2\left(B - \frac{1}{2}\right) - \left(B - \frac{1}{2}\right)$ $\frac{1}{2}\delta^2\widetilde{a}_1(t-1)=0$. Therefore, there exists $u_1(t-1)\in\mathbb{U}(u_1(t-1))$ so that $s_{\omega,1}(t)\geq 0$.

Furthermore, we need to consider a scenario/state transition under Scenario II. Specifically, if s-CAV(2) cuts in between s-CAV(1) and its follower, n-CAV(ω) at step t, Then, Scenario II transfers to the special one where s-CAV(2) follows s-CAV(1) and is followed by the n-CAV(ω). Accordingly, we need to prove the recursive feasibility of the constraints regarding s-CAV(2) in this special scenario. Mainly, we want to show $\mathscr{P}_u(u_2(t)) \cap \mathscr{P}_v(u_2(t)|\chi_1) = \mathbb{U}(u_2(t)) \neq \emptyset$, and then there exists $u_2(t) \in \mathbb{U}(u_2(t))$ such that $\mathscr{P}_u(u_2(t)) \cap \mathbb{P}_v(u_2(t)) = \mathbb{P}_v(u_2(t))$ $\mathscr{P}_{\gamma}(u_2(t)|\chi_3) \neq \varnothing$ given Conditions (i) – (iv) hold. By the same arguments about Case (1), we can show that $\mathbb{U}(u_2(t)) \neq \varnothing$. Next, as the cutting-in is carried out at step t, we have $\eta_{\omega,2}^r(t)=1$ and $\eta_{\omega,2}^r(t-1)=0$ (i.e., n-CAV(ω) starts to follow s-CAV(2) at step t but not t-1).

Accordingly, the safety constraint (27) makes the cut-in speed $v_2(t)$ satisfy $v_2(t) - \widehat{v}_{\omega}(t) \ge \frac{\widetilde{a}_2\delta(B-\frac{1}{2})}{A}$, which indicates Condition (iv) holds. Then following the similar discussion for s-CAV(1) under Scenario II, we can show that $s_{\omega,2}(t+1) \ge 0$ for any control input $u_2(t) \in \mathbb{U}$. The above arguments conclude that if s-CAV(1) is under Scenario II, the feasibility holds after the state transition. Wrapping up the derivations and arguments above, we complete the proof for Theorem 1.

Remark 1. Theorem 1 specifies the applicability of our MPC system. It indicates that the recursive feasibility only holds if the reaction time of HDVs satisfies $\tau_{\omega} \leq \overline{\tau}_{\omega} = \frac{-(v_{x}-5a_{x})-\sqrt{(v_{x}-5a_{x})^{2}-24a_{x}d_{\omega}}}{2a_{x}}$. Based on this mathematical formulation, we notice that $\overline{\tau}_{\omega}$ is closely related to the maximum deceleration of s-CAVs, \underline{a}_{x} , the speed limit \underline{v}_{x} and Newell's displacement d_{ω} . According to Manual (2000); Meng et al. (2021), we set the parameter values as follows, $\underline{v}_{x} = 5$ m/s, $d_{\omega} = 5$, and $\underline{a}_{x} = -6$ m/s^{2} , and then get $\overline{\tau}_{\omega} = 6.59$ s. Existing literature (Manual, 2000; Wei et al., 2017) shows that the normal operator and braking system reaction time, $\tau_{\omega} = 2.0$ s $\leq \overline{\tau}_{\omega} = 6.59$. Then, we claim that our MPC system will keep the recursive feasibility in most traffic scenarios. Furthermore, based on the CACC scheme of n-CAVs in (25), A and B can take different values depending on the value of control gain k_{2} . Our discussion of Condition (iv) above (55.2) indicates that the recursive feasibility only holds if B > 0.5 (or $k_{2} > 0.7s^{-1}$ when control time gap $t_{d} = 0.6s$). This analysis result suggests the range for the CACC control parameter within which our MPC is applicable. According to Xiao et al. (2017), k_{2} is set as $1.6s^{-1}$ to well fit the field data under the normal traffic and indicates our MPC system will hold the recursive feasibility in the normal traffic.

Remark 2. The sequential feasibility proof is closely related to the CACC scheme that *n*-CAVs adopt to control their movement. If they follow a CACC scheme different to the PATH model, the CAV dynamics (26) and equation set (54) will be substituted by the new CACC scheme formulation. Therefore, the speed of the *n*-CAV and its leading vehicle might follow a condition different from Condition (iv) in Theorem 1. In addition, we might end up with a safety lane-changing condition different from constraint (27). Accordingly, different algebra discussions may be required for the recursive feasibility proof. Nevertheless, we can still follow the same structure of the proof below (54) to examine the recursive feasibility with different CACC schemes. Mainly, we need to show that the spacing is positive built upon the new Condition (iv) and prove that the state transition is feasible under the new safety lane-changing condition.

7. Extensions: multiple vehicles synchronization

This section discusses extending/applying the synchronization control to the scenario that requires synchronizing more than two ($I \ge 3$) vehicles for certain applications, such as platoon formation. Recall that platoon formation often consists of two stages of decisions as follows: (1) determining which lane to form the platoon by what vehicle orders in the platoon; (2) planning the trajectories of vehicles to form the platoon according to the decisions made in the first stage. This multi-vehicle synchronization control fits in the trajectory planning stage. Namely, with a given target lane and vehicle order in the platoon, the synchronization control is able to guide multiple vehicles' movements to form the platoon. Below, we first introduce how to extend the MPC in (36) to adapt the control to multi-vehicle synchronization. Then, we transform the extended MPC into a more complicated hybrid MPC system to tackle the complexity of adaptive weighting raised by multi-vehicle and multi-objective control.

As mentioned above, multi-vehicle synchronization is built upon a given target synchronization lane and vehicle orders. Therefore, we consider a set of subject CAVs by the indices, $i \in I' = \{1, 2, ..., I\}$, seeking to form a platoon on target lane \widetilde{I} , in the order of 1, 2, ..., I. Without loss of generality, we consider an order that s-CAV(1) follows s-CAV(2), which follows s-CAV(3), and similarly, s-CAV(I-1) follows s-CAV(I). Based on the above information, MPC in (36) can be extended to the new MPC (57) with minor changes, adapting to multi-vehicle synchronization.

$$J(u_t) = \min \sum_{t=0}^{T-1} \frac{1}{2} \left[\underbrace{\mathbf{u}_t^T Q_{\mathbf{u}} \mathbf{u}_t}_{J_{\mathbf{u}}} + \underbrace{\mathbf{w}_t^T Q_{\mathbf{w}} \mathbf{w}_t}_{J_{\mathbf{w}}} - \underbrace{\mathbf{y}_t^T Q_{\mathbf{y}} \mathbf{y}_t}_{J_{\mathbf{y}}} - \underbrace{\widetilde{\eta}_t^T Q_{\bar{\eta}} \widetilde{\eta}_t}_{J_{\mathbf{v}}} + \underbrace{\mathbf{v}_t^T Q_{\mathbf{v}} \mathbf{v}_t}_{J_{\mathbf{v}}} \right] + \underbrace{q_z \mathbf{z}^T}_{J_z}$$

$$(57)$$

For, $t \in T$, $i \in I'$ s.t. (7) - (10), (12) –(21), and (25) - (35). where $\eta_{1-1,I}^{\bar{l}}(t)$. $\eta_{i,i'}^{\bar{l}}(t)$ defined in Eq. (3) indicates whether s-CAV(i) follows s-CAV(i') at timestep t. $J_{\bar{\eta}}$ represents the summation of variable $\eta_{1,2}^{\bar{l}}(t)$, $\eta_{2,3}^{\bar{l}}(t)$,..., $\eta_{I-1,I}^{\bar{l}}(t)$. Compared to the MPC in (36) working for two s-CAVs, the new MPC in (57) enables more than two s-CAVs synchronization by modifying J_{η} to $J_{\bar{\eta}}$ such that the objective function rewards the duration that all s-CAVs of interest are driving in the given order on the target lane, \tilde{l} . On the other hand, different from two-vehicle synchronization, the new MPC in (57) should not be simply decomposed into two sequential MPCs introduced in Section 5.1 since it involves multiple catch-up and platooning states. Consequently, we introduce a complicated hybrid MPC system that sequentially decomposes the MPC in (57) according to the car-following relationship of multiple s-CAVs pairs. We present this modification as follows.

Recall that Section 5.1 decomposes the MPC into two sequential MPC-I and MPC-II to facilitate the adaptive weighting schemes that balance synchronization efficiency and traffic impacts. Specifically, MPC-I instructs two s-CAVs to approach each other quickly (or in the catch-up state), and MPC-II focuses on stabilizing the movement (i.e., spacing) of two s-CAVs when one is already following the

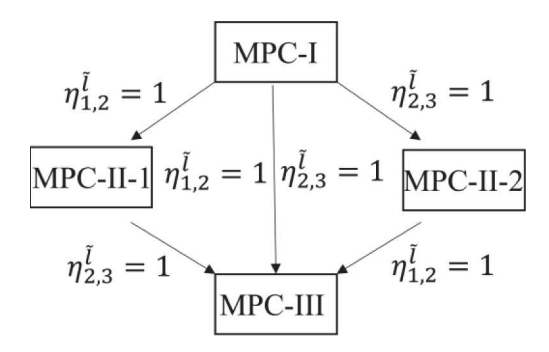


Fig. 3. Hybrid MPC system for multiple subject CAVs synchronization.

other (or in the platooning state). Following the same thought, any pair of s-CAVs in the multi-vehicle synchronization scenario can either be in the catch-up or platooning state. Moreover, the state transition does not occur in a predetermined order due to traffic uncertainty. Therefore, we design a hybrid MPC system that dynamically decomposes the new MPC according to the state of the s-CAV pairs. For simplicity of the presentation, we present the idea of this hybrid MPC system by a three-CAV synchronization scenario shown in Fig. 3.

Without loss of generality, we consider that the system starts with the state that all s-CAVs try to catch up. Then, the MPC-I in (58) only including the objectives in J_u to $J_{\bar{\eta}}$ (excludes J_e and J_x) is implemented for the synchronization control to encourage pairs of s-CAV to transform to the platooning state promptly.

7.1. MPC-I

$$Min \ \Gamma_{1}(\mathbf{u}_{t}) = \sum_{t=0}^{T-1} \frac{1}{2} \left[\underbrace{\mathbf{u}_{t}^{T} Q_{\mathbf{u}} \mathbf{u}_{t}}_{J_{\mathbf{u}}} + \underbrace{\mathbf{w}_{t}^{T} Q_{\mathbf{w}} \mathbf{w}_{t}}_{J_{\mathbf{w}}} - \underbrace{\mathbf{y}_{t}^{T} Q_{\mathbf{y}} \mathbf{y}_{t}}_{J_{\mathbf{y}}} - \underbrace{\widetilde{\eta}_{t}^{T} Q_{\overline{\eta}} \widetilde{\eta}_{t}}_{J} \right]$$

$$(58)$$

For, $t \in T$, $i \in I$'s.t. (7) - (10), (12) - (21), and (25) - (35).

Next, according to the given vehicle order, one of the two target short platoons each involving two s-CAVs will be formed first during sychronizaton process: either s-CAV(1) and s-CAV(2) or s-CAV(2) and s-CAV(3). If the pair of s-CAV(1) and s-CAV(2) goes first, we will have $\eta_{1,2}^{\tilde{l}}(t)=1$, which triggers the MPC-I to switch to MPC-II-1 in (59) accordingly. It focuses on maintaining a desired spacing between s-CAV(1) and s-CAV(2), synchronizing their speed through the item J_{ν} (using $Q_{\nu}^{1,2}$), and encouraging s-CAV(2) and s-CAV(3) to establish the platooning state through the item $J_{\tilde{\eta}}$ (using $Q_{\tilde{\eta}}^{2,3}$). Similarly, if the pair of s-CAV(2) and s-CAV(3) switches to the platooning state first, the MPC-I will switch to MPC-II-2, which is similar to MPC-II-1 but encourages s-CAV(1) and CAV(2) to form a platoon by the item $J_{\tilde{\eta}}$ (using $Q_{\tilde{\eta}}^{1,2}$) and synchronizes the speed of s-CAV(2) and s-CAV(3) by J_{ν} (using $Q_{\nu}^{2,3}$).

7.2. MPC-II-1

$$Min \ \Gamma_2(u_t) = \sum_{t=0}^{T-1} \frac{1}{2} \left[\underbrace{\mathbf{u}_t^T Q_{\mathbf{u}} \mathbf{u}_t}_{J_{\mathbf{u}}} + \underbrace{\mathbf{w}_t^T Q_{\mathbf{w}} \mathbf{w}_t}_{J_{\mathbf{w}}} - \underbrace{\mathbf{y}_t^T Q_{\mathbf{y}} \mathbf{y}_t}_{J_{\mathbf{y}}} + \left(- \underbrace{\widetilde{\eta}_t^T Q_{\bar{\eta}} \widetilde{\eta}_t}_{J_{\bar{\eta}}} + \underbrace{\mathbf{v}_t^T Q_{\mathbf{v}} \mathbf{v}_t}_{J_{\mathbf{y}}} \right) \right] + \underbrace{q_z \mathbf{z}^T}_{J_z}$$

$$(59)$$

For, $t \in T$, $i \in I'$

s.t.
$$\eta_{1,2}^{\tilde{l}}(t) = 1, t \in T$$

(7) - (10), (12) - (21), and (25) - (35).

Finally, when all s-CAVs are in platooning state following the predefined vehicle order, the synchronization control is switched to the MPC-III in (60), which focuses on maintaining the spacing of all pairs of s-CAVs to the desired spacing and synchronizing their speed.

³ It is possible that s-CAV(1) and s-CAV(3) forms a platoon during the synchronization process. If this happens, we consider it as a catch-up state since s-CAV(1) and s-CAV(3) is not the designed order for the platoon formation.

Table 2 Parameter settings for experiments.

Parameters	Values
MPC prediction horizon T	5 (sec)
Sample time interval δ	1 (sec)
Vehicle length L_i	5 (m)
Maximum speed $\overline{\nu_x}$	33.33 (m/s)
Minimum speed v_x	10 (m/s)
Acceleration limit $\overline{a_x}$	$8 (m/s^2)$
Deceleration limit a_x	$-6 \text{ (m/s}^2\text{)}$
Jam density $k_c^{l,max}$	0.12 (veh/m)
Cell capacity $q_c^{l,max}$	2000 (veh/h)
Cell length ΔL	40 (m)
Maximum weighting bound, $\xi_{max}^{I}(\xi_{max}^{II})$	10
s-CAV detection range	150 (m)

7.3. MPC-III

$$Min \Gamma_{2}(\mathbf{u}_{t}) = \sum_{t=0}^{T-1} \frac{1}{2} \left[\underbrace{\mathbf{u}_{t}^{T} Q_{\mathbf{u}} \mathbf{u}_{t}}_{J_{\mathbf{u}}} + \underbrace{\mathbf{w}_{t}^{T} Q_{\mathbf{v}} \mathbf{w}_{t}}_{J_{\mathbf{v}}} - \underbrace{\mathbf{y}_{t}^{T} Q_{\mathbf{v}} \mathbf{y}_{t}}_{J_{\mathbf{v}}} + \underbrace{\mathbf{v}_{t}^{T} Q_{\mathbf{v}} \mathbf{v}_{t}}_{J_{\mathbf{v}}} \right] + \underbrace{q_{z} \mathbf{z}^{T}}_{J_{z}}$$

$$(60)$$

For, $t \in T$, $i \in I'$

s.t.
$$\eta_{1,2}^{\tilde{l}}(t) = 1, \eta_{2,3}^{\tilde{l}}(t) = 1, t \in T$$

The above discussion provides a decomposition strategy of the hybrid MPC system for three-vehicle synchronization. If there are I s-CAVs and the vehicle order of the platoon is predetermined, then there are (I-1) short platoons, each invovling two s-CAVs, in the formed platoon. We define these short platoons as target s-CAV pairs. Each such target s-CAV pair can be in either catch-up state or platooning state. Based on these two states, the MPC (57) can be transformed into a hybrid MPC system consisting of three types of MPC. Specifically, MPC-I is implemented when all target s-CAV pairs are in a platooning state with predefined vehicle order, and MPC-II is used when platooning state and catch-up state are mixed for such a s-CAV pairs. Specifically, there are (I-1) customized MPC-II, each of which has a similar format but factoring different pairs of s-CAVs in the items of $J_{\tilde{\eta}}$ and J_c in (59). These MPC-IIs transform from one to another whenever there is a target s-CAV pair transforming from the catch-up state to target platooning state. In summary, a path in the hybrid MPC system starts from MPC-I, transforms to one and another MPC-II due to traffic uncertainty, and finally switches to MPC-III. Built upon the above discussions, we claimed that the hybrid MPC system can be generalized for more-than-three-vehicle cases.

8. Experiments

This section conducts three sets of numerical experiments to validate the efficiency of the synchronization control, demonstrate the merits of the adaptive weighting strategy, and investigate the effects of traffic congestion level and CAV penetration rate on the performance of the synchronization control.

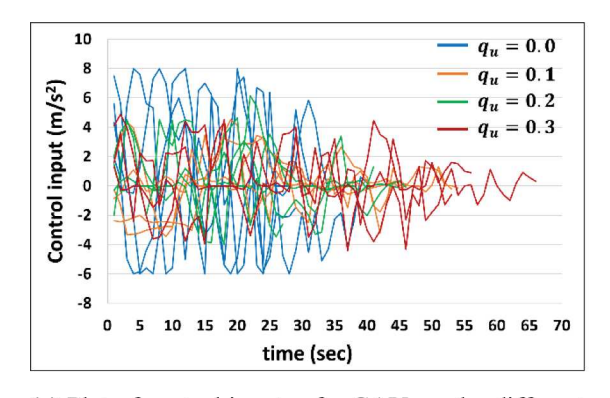
The experiments are built upon the NGSIM data collected on the eastbound of the I-80 in San Francisco Bay at Emeryville, California, 4:00 pm to 4:15 pm on April 15, 2005. The testbed provides vehicle trajectory information, including lane membership, position, speed, and acceleration. We randomly select 3-lanes road segments in the testbed to generate 150 testing cases. Among the vehicles in each testing case, we randomly choose two vehicles as the subject CAVs and label the other vehicles as neighbor vehicles. The initial conditions of all vehicles as well as the trajectory profiles of leading HDVs are sampled from NGSIM data. Meanwhile, we test the CAV penetration varies from 0% to 100% with 10% as step size. Correspondingly, a proportion of the neighbor vehicles are considered as neighbor CAVs for each experiment based on the predetermined CAV penetration rate. All the experiments share the default setting for some parameters presented in Table 2 according to NGSIM field data and Police Radar Information Center (2020). All experiments are run on a DELL Precision 3630 Tower with 3.60 GHz of Intel Core i9–9900k CPU, 8 cores and 16 GB RAM in a Windows environment.

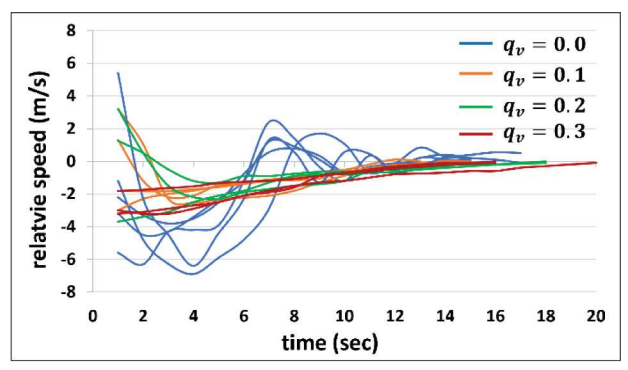
8.1. Performance of synchronization control with adaptive weighting strategies

We first demonstrate the performance of the synchronization control with a particular interest in showing the merit of the adaptive weighting strategy. Before presenting our experiment results, we first explain the measurement metrics used in this experiment. It is slightly different from the measurements we used in the mathematical model but provides a consistent evaluation of the performance.

Table 3 Values of weights for each strategy.

MPC-I				
	Balanced (S1)	Synchronization dominant (S2)	Traffic dominant (S3)	Adaptive weighting
q_{η}	0.40	0.40	0.20	Adaptive
$q_{i,w}$	0.40	0.20	0.40	0.40
MPC-II				
q_z	0.35	0.35	0.15	Adaptive
$q_{i,\omega}$	0.35	0.15	0.35	0.35





- (a) Plot of control inputs of *s*-CAVs under different control weights (MPC-I & MPC-II)
- (b) Plot of relative speed of *s*-CAVs under different weights (MPC-II only)

Fig. 4. Plot of control inputs (traffic smoothness) and relative speed (speed harmonization) under different weights.

Recall the MPC in (36) measures the traffic performance by (i) traffic smoothness; (ii) *s*-CAVs' speeds; (iii) upstream traffic propagation. Accordingly, this experiment collects the *average traffic speed* involving both *s*-CAVs' neighbor vehicles and the upstream traffic under the synchronization control. It consistently reflects the traffic efficiency in terms of items (ii) and (iii) in the MPC. The synchronization control's impact on traffic smoothness is examined by the fluctuation of control inputs of *s*-CAVs. The smoother s-CAV movements cause less traffic fluctuation. Meanwhile, the synchronization performance under the MPC in (36) is also measured from three aspects, including (i) speed harmonization; (ii) the time that it takes for *s*-CAVs to be positioned in car-following mode; (iii) the time that it takes to stabilize the *s*-CAVs' spacing. Accordingly, the experiments collect the total time to complete the synchronization (sum of (ii) and (iii)) to demonstrate the synchronization efficiency. The speed harmonization reflects how much we stabilize the speed of the two *s*-CAVs. It can also be evaluated by the variation of the relative speed between the two *s*-CAVs.

On the other hand, to implement the experiments, we need to determine the weights of the multi-objective function of the optimizer used in the MPC. Recall that our weighting strategy adaptively tunes q_{η} in MPC-I or q_{ε} in MPC-II (see Eqs. (41) and (43)), but keep the weights q_u for traffic smoothness and q_{ε} for the speed harmonization constant since they are consistently important during the entire synchronization control. Accordingly, before showing the merits of our adaptive weighting strategy, our experiments first want to learn the proper values for q_u and q_{ε} . To do that, the experients first screen the values of q_u (and q_{ε}) with the step size 0.1, while using adaptive weighting strategy for other weights according to the settings in Table 3.

Fig. 4 plots the control inputs and relative speed of s-CAVs in some randomly picked cases. Fig. 3(a) indicates that 0.1 is the proper value for q_u . More exactly, this setting smoothens the movements of s-CAVs and leads to less traffic fluctuation as compared with the setting: $q_u = 0.0$. On the other hand, further increasing q_u to 0.2 and 0.3 does not significantly improve the smoothness of s-CAVs' movements but results in a longer time to complete synchronization. Fig. 3(b) demonstrates that $q_e = 0.1$ works resonably well to synchronize the relative speed (less relative speed variations), when the two s-CAVs are already positioned in the car-following mode (under MPC-II) and seek to stabilize their spacing and relative speed. We do not see the further improvement in the speed harmonization by increasing q_e to 0.2 and 0.3.

With the hint from Fig. 4, we put both q_u and q_v equal to 0.1 to examine the effectiveness of the adaptive weighting strategy. Specifically, we compare the comprehensive performance of the synchronization control under four weighting strategies: (i) the balanced strategy (S1-bal), which considers traffic and synchronization efficiency equally important and sets q_{η} and $q_{i,w}$ in MPC-I (or q_x and $q_{i,w}$ in MPC-II) with even weights in the objective function; (ii) the synchronization dominant strategy (S2-syn), which prioritizes the synchronization over the traffic efficiency by setting a larger value for q_{η} than for $q_{i,w}$ (or a larger value for q_x than for $q_{i,w}$ in MPC-II); (iii) the traffic dominant strategy (S3-trf), which overweighs the traffic efficiency; (vi) the adaptive weighting strategy according to Eqs. (41) and (43), for which we further test how the tunable parameter α affects its performance. The values of weights for all the weighting strategies are presented in Table 3.

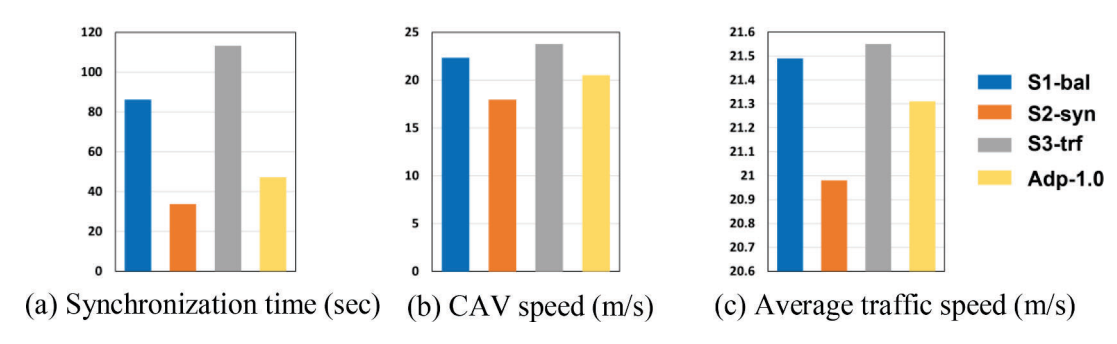


Fig. 5. Comparison of traffic and synchronization efficiency under different weighting strategies.

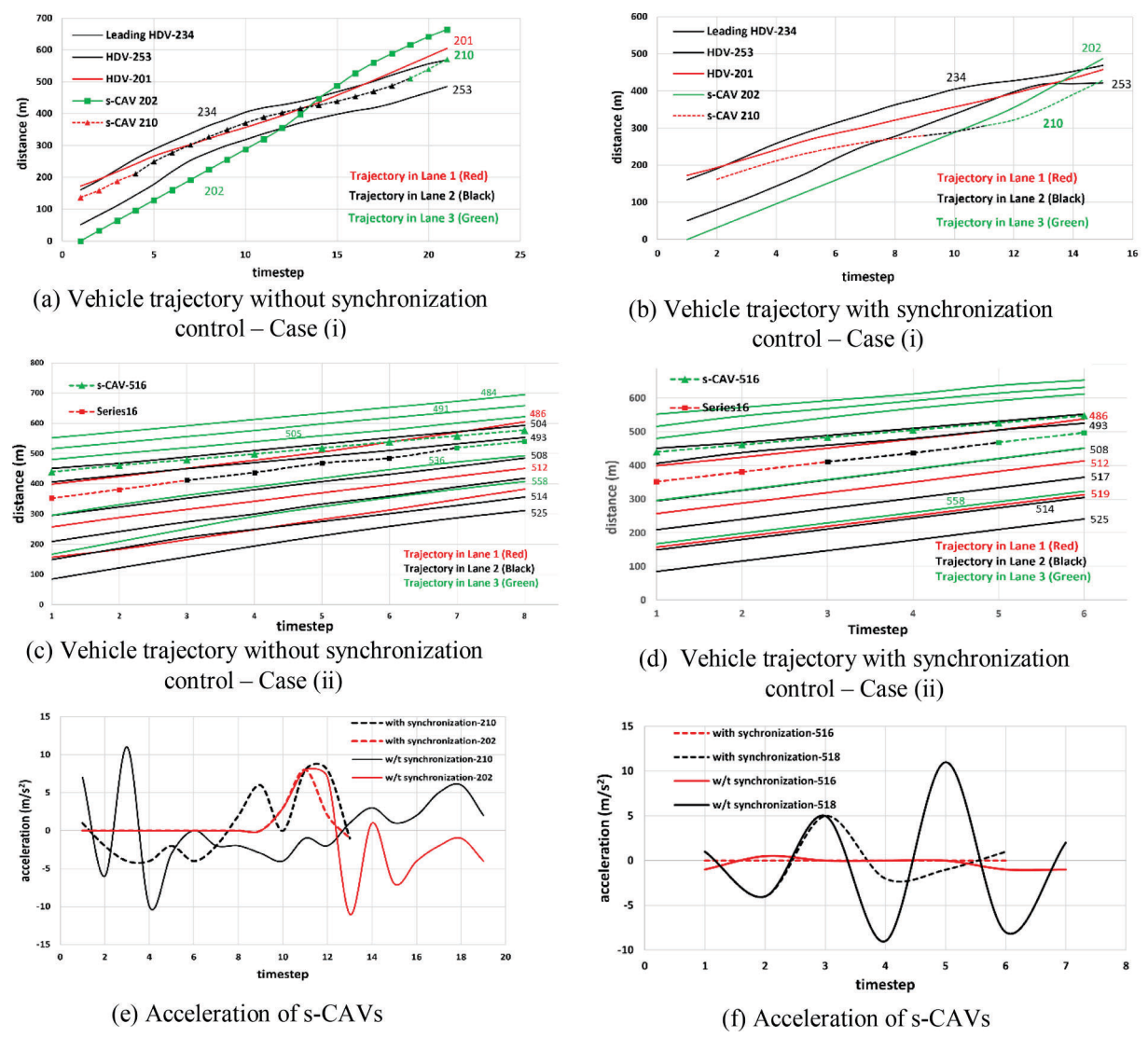


Fig. 6. Vehicle trajectories without and with synchronization control for Case (i) ((a) and (b)) and Case (ii) ((c) and (d)); Acceleration of s-CAVs for Case (i) (e) and Case (ii) (f).

Fig. 5 demonstrates the results regarding time to complete the synchronization, s-CAV speed and average traffic speed under the weighting strategies. It can be observed that strategy S2-syn makes the synchronization complete fastest as expected, i.e., 33.74 s. But, it significantly slows down s-CAVs' speed (17.95 m/s on the average) and the surrounding traffic's speed (20.98 m/s on the average).

Table 4 Synchronization performance with and without synchronization control.

	Performance metrics			
	Iincrease of s-CAV speed (%)	Increase of neighbor vehicle speed (%)	Reduction of synchronization completion time (%)	Reduction of s-CAV acceleration fluctuation (%)
Case (i)	1.3%	8.1%	28.6%	27.5%
Case (ii)	3.8%	0.9%	37.5%	55.2%

Table 5Average vehicle speeds without and with synchronization control.

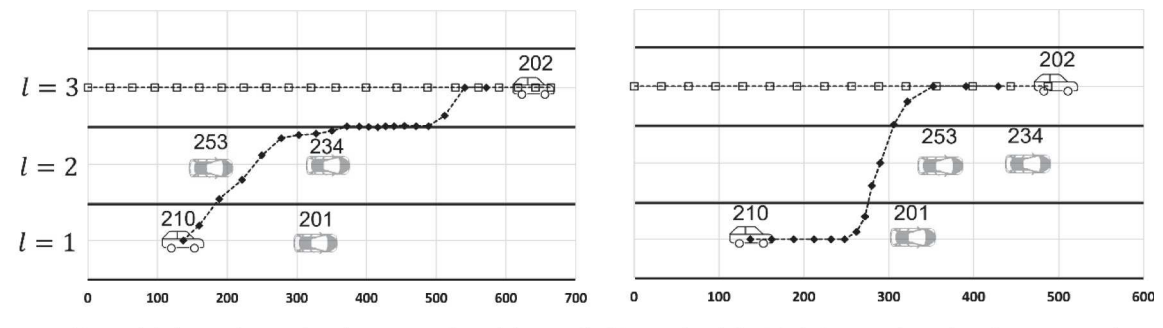
Case (i)			
Vehicle ID	Speed without synchronization control (m/s)	Speed with synchronization control (m/s)	
202	33.19	34.81	
210	21.73	20.85	
Neighboring vehicles	21.22	22.93	
Case (ii)			
Vehicle ID	Speed without synchronization control (m/s)	Speed with synchronization control (m/s)	
516	19.85	21.58	
518	26.45	26.50	
Neighbor vehicles	27.05	27.28	

On the other hand, strategy S3-trf enables s-CAVs and the surrounding traffic to move fastest (23.78 m/s and 21.55 m/s on average, respectively). Still, it takes the longest time to have s-CAVs complete the synchronization (113.25 s). We can also observe that strategy S1-bal performs better than strategy S3-trf by evenly considering the time to complete the synchronization and traffic speed. More specifically, under strategy S1-bal, we can significantly reduce the synchronization time by 23.9% (from 113.25 s under S3-trf to 86.14 s under S1-bal) with minor sacrifice in average traffic speed (i.e., reduce 0.3% from 21.55 m/s under S3-trf to 21.49 m/s under S1-bal). However, S1-bal is not perfect. It makes the synchronization take a much longer time to complete than that under the strategy S2-syn (86.14 s vs. 33.74 s). On the other hand, as compared with strategy S1-bal, the adaptive weighting strategy enables the controller to trade a bit of average speed to significantly reduce the time needed to complete the synchronization. Recall that the weights q_{η} in MPC-I (and q_{s} in MPC-II) are associated with the synchronization performance metrics and they are adaptively tuned according to Eqs. (41) and (43), in which α represents the tuning level. For example, larger α gives larger weight on q_{η} and q_{s} , which promotes the synchronization process. We tested different values of α and found that the performance of adaptive weighting strategy will not significantly change when $\alpha > 0.5$. As a result, we present the result under $\alpha = 1.0$ in Fig. 5. The yellow column in Fig. 5 indicates that under the adaptive weighting strategy (Adp-1.0), the controller trades 0.84% average speed reduction (from 21.49 m/s under S1-bal to 21.31 m/s) for a significant reduction in the time to complete the synchronization (from 86.14 s (S1-bal) to 47.12 s). Therefore, we conclude that the developed adaptive weighting strategy outperforms other weighting methods that have fixed weights.

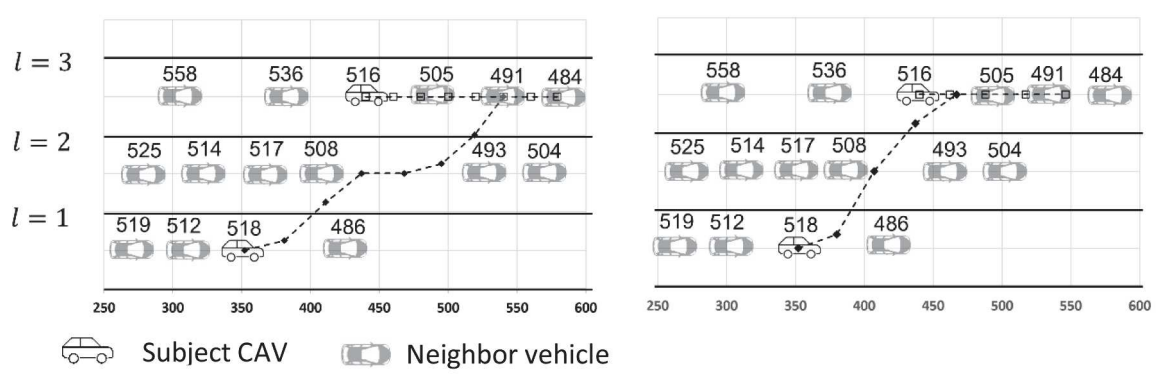
8.2. Synchronization control effectiveness

Next, this study demonstrates the effectiveness of the synchronization control by comparing it to two field cases in NGSIM field dataset. Each case has different initial conditions, i.e., number of neighbor vehicles and their initial positions. To be noted, these experiments only considered the two selected subject vehicles as CAVs to implement our synchronization control, and all other neighboring vehicles were HDVs. Therefore, no n-CAVs involved in this effect so that we can screen out the effect of the CACC scheme. In each case, we observed that a vehicle conducted several lane-changing and then stabilized a following mode behind the other vehicle. Even though we have no data to specify the real purpose of this movement, we consider this to be a synchronization process without implementing a cooperative control and use it as a benchmark to demonstrate the traits of our approach. Fig. 7 plots the trajectories of subject vehicles (ID = 210, 202 in Case (i) and ID = 518, 516 in Case (ii)) with 1.0 s resolution from NGSIM field data (without synchronization, left) and under the synchronization control (right). The neighboring vehicles are labeled with corresponding IDs. To better evaluate the results, we plot the vehicle trajectories of s-CAVs and neighbor vehicles in Fig. 6(a) – (d) as well as the control inputs (acceleration) of s-CAVs in Fig. 6(e)–(f). Moreover, to demonstrate the significance of the improvement, we summarized the percentage performance improvement of synchronization control in Table 4 from multiple perspectives, and presented the average speeds of neighboring and subject vehicles without and with synchronization control in Table 5.

More exactly, Case (i) in Fig. 7(a) provides an example under a sparse traffic only involving 5 vehicles. Fig. 7(a, left) shows that subject vehicle 210 in Case (i) initially drove on lane 1, moved from lane 1 to lane 3, and eventually approached vehicle 202 in lane 3. The process involved two lane changes, and affected three neighboring vehicles, and took 20 s to complete. Assuming Case (i) is an example of a catch-up maneuver, vehicles 210 and 202 are the subject CAVs. Fig. 7(a, right) provides the trajectory under the synchronization control. We can observe that vehicle 210 no longer cut in between vehicle 253 and vehicle 234 on lane 2, which very



(a) Vehicle trajectories in Case (i) without (left), and with (right) synchronization control.



(b) Vehicle trajectories in Case (ii) without (left), and with (right) synchronization control.

Fig. 7. Comparison of vehicle trajectories without and with synchronization control (x-axis; horizontal coordinate of the vehicle in meters).

likely blocks the traffic. Instead, it stayed in lane 1 until it had a loose space to move to lane 2. After that, it stayed in lane 2, followed vehicle 253 for a while, and eventually moved to lane 3 to catch vehicle 202 when it was close. Table 4 and Fig. 6(a) and (b) show that both the two subject vehicles and the neighboring vehicles drive faster under the synchronization control than they did without synchronization control (in the field). Fig. 6(e) shows that the acceleration of s-CAVs are smoother under synchronization control. These results demonstrate the efficiency and effectiveness of the synchronization control.

Case (ii) involves a similar "catch-up" motion between vehicle 518 and vehicle 505 under congested traffic. It affects 16 vehicles within 8 s. The dash-dot lines in Fig. 7(b) show the trajectories of vehicle 518 observed without synchronization control (the field data) and the simulation under the synchronization control. Even though they both involve two lane-changing maneuvers, our experiment data indicated that the synchronization took much less time (3 s) to complete under the synchronization control than it initially did (8 s). Moreover, Table 4 and Fig. 6(c) and (d) demonstrate a similar improvement in traffic efficiency to Case (i). These improvements in traffic and synchronization confirm the value of the complicated MPC factoring in hybrid traffic dynamics in the trajectory control. Finally, by comparing Case (ii) to Case (i), we noticed that even though Case (ii) involves more neighbor vehicles than Case (i), the corresponding synchronization takes less time to complete than it does in Case (i) under sparse traffic. This result indicates that besides the number of neighbor vehicles and traffic congestion level, the initial position of s-CAVs also plays an important role in the synchronization performance.

8.3. Sensitivity analysis

The results from the last section indicate that the synchronization control performance is affected by the congestion level, CAV penetration, and the initial positions of the two s-CAVs. This section conducts the sensitivity analysis to investigate their effects. Our experiments screened the synchronization efficiency and traffic efficiency under different traffic congestion levels represented by the traffic volume (ν) to capacity (c) ratio (v/c)⁴ varying from 0.35 to 0.85 and different CAV penetration ranging from 0% to 100% with the step size equal to 10%. We ran the experiments in multiple cases for each scenario with a given congestion level and CAV penetration, each of which randomly selects the initial positions of the two subject CAVs. Below we discuss the experiment results.

⁴ Please refer to Appendix C for a detailed discussion on the calculation of v/c.

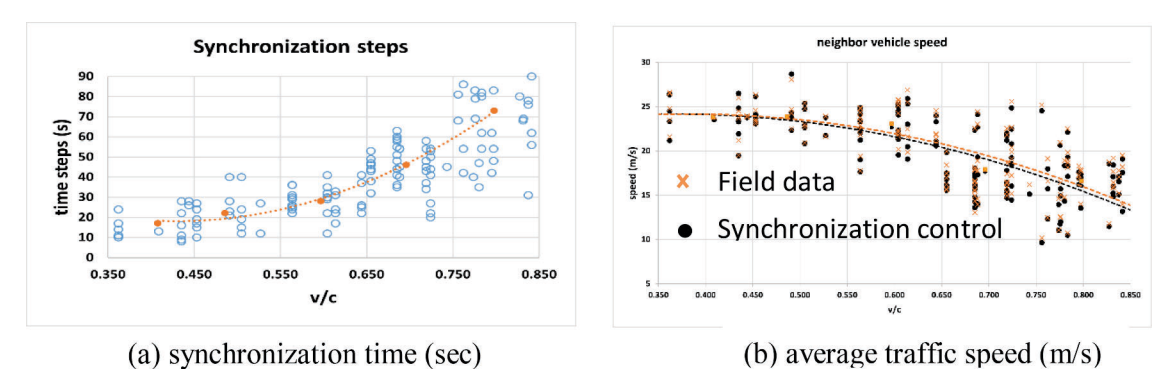


Fig. 8. Performance of synchronization control under different congestion levels.

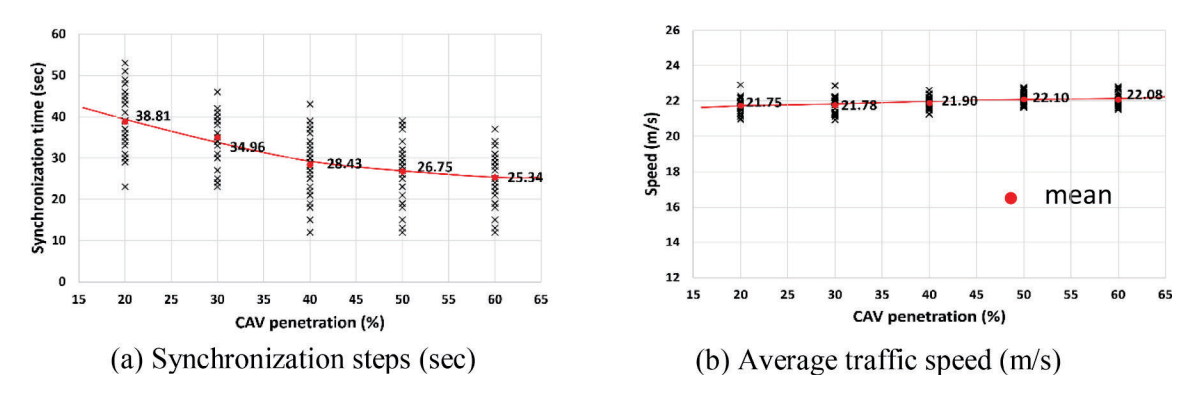


Fig. 9. Performance of synchronization control under different CAV penetration rate.

8.3.1. Impact of traffic congestion

We first tested the impact of congestion levels on the synchronization control performance. Our screening experiments show that raising CAV penetration will generally benefit the synchronization control performance, but its marginal effect diminishes and becomes insensitive after 50%. To highlight the impact of traffic congestion levels, below we present the results under 50% CAV penetration in this subsection.

Fig. 8 plots the time to complete the synchronization (i.e., synchronization time in Fig. 6(a)) and the average traffic speed of the testing cases under different congestion levels. Specifically, Fig. 6(b) compares the average vehicle speed of neighbor vehicles under synchronization control and without synchronization operation (field data). Fig. 8(a) indicates that the time steps needed to complete the synchronization control increases gradually when the traffic v/c ratio is below 0.55 (i.e., under light and mildly congested traffic), and then rises significantly as v/c ratio increases further (i.e., under congested and highly congested traffic). This is reasonable. When the traffic is congested, the two s-CAVs need more time to manage their movements (e.g., lane changes, acceleration/deceleration) and then approach each other, given neighbor vehicles move slowly. On the other hand, Fig. 8(b) shows the average speed of surrounding traffic with the synchronization control in our simulation (the black curve) is very close to the corresponding field traffic speed without synchronization control (the orange curve). Therefore, we confirm that this synchronization control does not worsen traffic in most cases under different congestion levels. The negative effect only occurs slightly when traffic is highly congested such as v/c > 0.8. This observation is consistent with the findings in Section 8.2. Overall, the sensitivity analyses demonstrate that traffic congestion will slow down the synchronization process, but the synchronization control can well preserve traffic efficiency under different traffic congestion levels.

8.3.2. Impact of CAV penetration

Next, this study examines how CAV penetration affects the performance of synchronization control. The above experiments have shown that raising the congestion level will generally worsen the synchronization efficiency. This effect becomes significant when v/c ratio is above 0.55. To highlight the impact of the CAV penetration, Fig. 9 below presents the results of the cases with v/c varying between 0.45 to 0.55 (Note that the v/c is coming from the testing cases from field data. Under each penetration, we try to find the testing cases from the data with the v/c ratio ranging 0.45 to 0.55.)

From Fig. 9(a), we first observed that the time steps to complete the synchronization vary very much in the testing cases with different s-CAVs' initial positions even under the same CAV penetration, this observation renders the variation of the difficulties in synchronizing the two s-CAVs' movement. More exactly, Fig. 9(a) shows that the time needed to complete the synchronization decreases when the CAV penetration increases. We also observed that this positive effect is marginally diminishing. For instance, the

Neighbor vehicle speed under different communication ranges

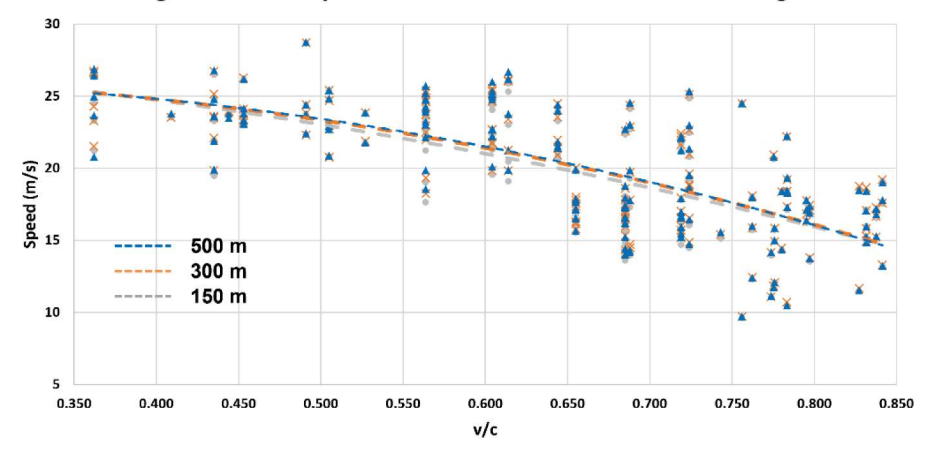


Fig. 10. Performance of synchronization control under different communication ranges.

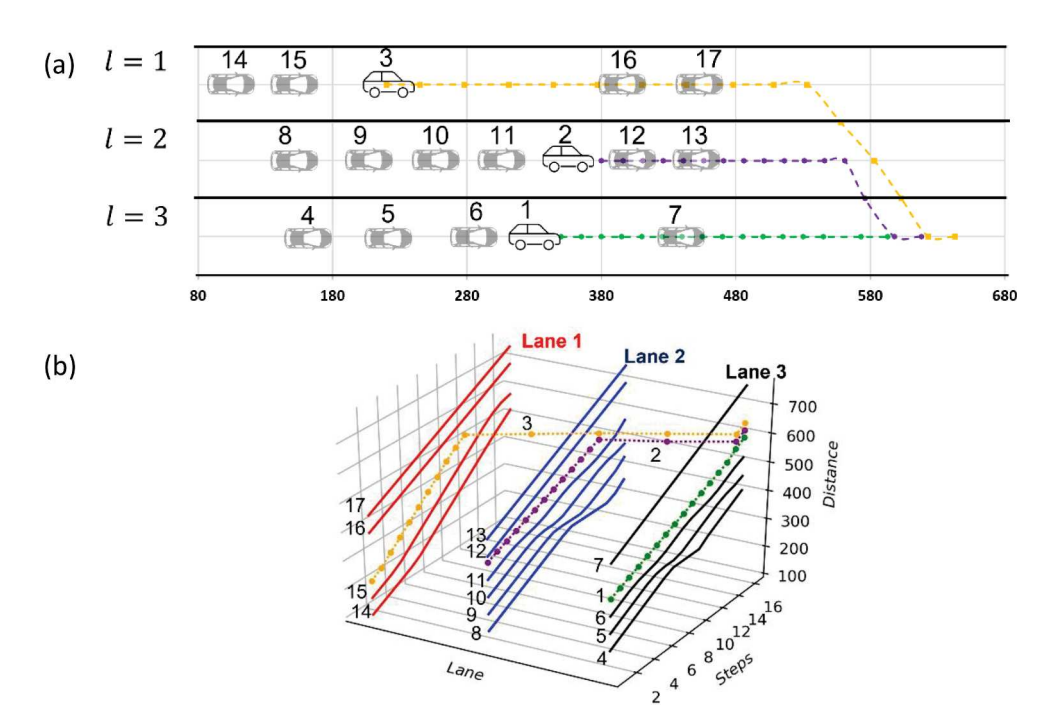


Fig. 11. Case study of three-vehicle synchronization. (a) Schematic representation of a three-vehicle synchronization example. (b) Vehicle trajectories of three subject CAVs.

mean time to complete the synchronization control is significantly reduced 27% from 38.81 s to 28.43 s when the CAV penetration increases from 20% to 40%. But it only reduces 11% from 28.43 s to 25.34 s as the CAV penetration increases from 40% to 60%. Fig. 9 (b) also shows that the average traffic speed increases 1.5% from 21.75 m/s to 22.08 m/s as CAV penetration increases from 20% to 60%. Moreover, our experiments observed that s-CAVs can complete the lane change more promptly if the neighboring vehicles are mainly CAVs rather than HDVs. Therefore, we confirm that CAVs' quicker response to s-CAV movement will benefit the synchronization control performance than HDVs do. Accordingly, more CAVs present in the background traffic make the synchronization control performance better.

8.3.3. Impact of communication range

This section investigated how the communication range, i.e., the distance between s-CAVs to trigger the synchronization control, affects the performance of synchronization control. According to Figure 17 in Maglogiannis et al. (2021), and Fig. 5 in (Ho et al., 2010), the communication range for C-V2X and DSRC are up to 500 m and 300 m, respectively, with 100% packet delivery rate. We also found recent studies widely adopted a communication range of 100–500 m (Shao and Sun, 2020; Sun et al., 2022) for V2V communication.

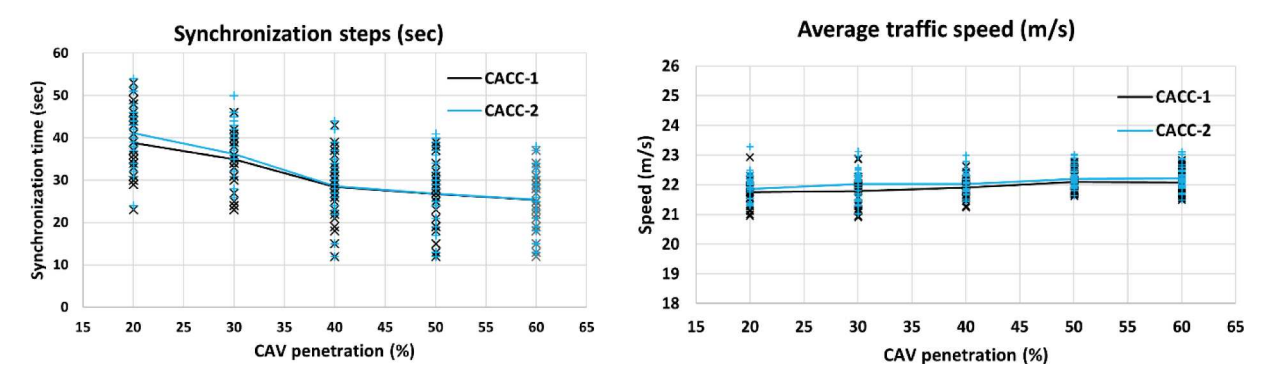


Fig. 12. Performance of synchronization control under different CAV penetration rate with different CACC scheme.

Table 6 Spacing between HDV(ω) and s-CAV(1).

Time (t)	0	k	2k	3k
$x_i(t)$	$s_{\omega,i}$	$s_{\omega,i} + u_i au_\omega + rac{1}{2} u_1(t) au_\omega^2$	$s_{\omega,i} + 2v_i \tau_\omega + 2u_1(t) \tau_\omega^2$	$s_{\omega,i}+3 u_i au_\omega+rac{9}{2}u_1(t) au_\omega^2$
$\widehat{\mathbf{x}}_{\omega}(t)$	0	$v_i au_\omega$	$\nu_i \tau_\omega + s_{\omega,i} - d_\omega$	$ u_i au_\omega+2s_{\omega,i}-2d_\omega+rac{1}{2}u_1(t) au_\omega^2$
$v_i(t)$	ν_i	$v_i + u_1(t) \tau_{\omega}$	$v_i + 2u_1(t)\tau_{\omega}$	$v_i + 3u_1(t)\tau_{\omega}$
$\widehat{\mathcal{V}}_{\omega}(t)$	v_i	$(s_{\omega,i}-d_\omega)/ au_\omega$	$\left(s_{\omega,i}-d_\omega+rac{1}{2}u_1(t) au_\omega^2 ight)igg/ au_\omega$	$(v_i au_\omega + 2u_1(t) au_\omega^2)/ au_\omega$
$s_{\omega,i}(t)$	$s_{\omega,i}$	$s_{\omega,i}+rac{1}{2}u_1(t) au_\omega^2$	$\nu_i\tau_\omega+2u_1(t)\tau_\omega^2+d_\omega$	$2v_{i}\tau_{\omega}-s_{\omega,i}+4u_{1}(t)\tau_{\omega}^{2}+2d_{\omega}$
$\Delta s_{\omega,i}(t)$		-	_	_
Time (t)	4k		5 <i>k</i>	6 <i>k</i>
$x_i(t)$	$s_{\omega,i} + 4v_i \tau_\omega + 8u_1(t) \tau_\omega^2$		$s_{\omega,i}+5 u_i au_\omega+rac{25}{2}u_1(t) au_\omega^2$	$s_{\omega,i}+6v_i\tau_\omega+18u_1(t)\tau_\omega^2$
$\widehat{x}_{\omega}(t)$	$2v_i au_\omega+2s_{\omega,i}-2d_\omega+rac{5}{2}u_1(t) au_\omega^2$		$4v_i au_\omega+s_{\omega,i}-d_\omega+rac{13}{2}u_1(t) au_\omega^2$	$6\nu_i\tau_\omega+12u_1(t)\tau_\omega^2$
$v_i(t)$	$v_i + 4u_1(t)\tau_{\omega}$		$v_i + 5u_1(t)\tau_{\omega}$	$v_i + 6u_1(t)\tau_{\omega}$
$\widehat{\mathcal{V}}_{\omega}(t)$	$(2v_i au_\omega-s_{\omega,i}+d_\omega+4u_1(t) au_\omega^2/ au_\omega$		$\left(2 u_i au_\omega - s_{\omega,i} + d_\omega + rac{11}{2} u_1(t) au_\omega^2 ight) igg/ au_\omega$	$(v_i \tau_\omega + 6u_1(t)\tau_\omega^2)/\tau_\omega$
$s_{\omega,i}(t)$.	$2v_i\tau_\omega-s_{\omega,i}$	$+\frac{11}{2}u_1(t) au_\omega^2+2d_\omega$	$\nu_i\tau_\omega+6u_1(t)\tau_\omega^2+d_\omega$	$s_{\omega,i} + 6u_1(t)\tau_\omega^2$
$\Delta s_{\omega,i}(t)$	_	4	_	+

Accordingly, we tested the synchronization control by extending the transmission range from 150 m to 300, and 500 m.

The results presented in Fig. 10 indicated that extending the communication range in the experiment from 150 to 300 m led to minor performance improvement; the effect become more invisible as it was extended from 300 to 500 m. Given that a longer range adds more computation load, we would recommend triggering the synchronization control when the distance between two vehicles is within 150 m. This result is consistent with the motivation of this study to develop a hybrid micro-macro model. The hybrid model consists of the "micro" moving dynamics model to describe the movement of each neighboring vehicles of the subject CAVs, and the "macro" traffic flow model to capture the traffic impact that propagates on the distant upstream traffic. Given that the hybrid model already has the capability to capture the out-of-range traffic impact, we do not expect the "micro" model to cover a longer range of traffic. Therefore, it is not necessary to set a long communication range to start the synchronization control.

8.4. Case study: three-vehicles synchronization

Next, we conducted experiments to demonstrate the capability of the synchronization control for more-than-two-vehicle synchronization. These experiments were built upon an example of three-vehicle synchronization with a given target lane l=3 agreeing with an order that s-CAV(1) follows s-CAV(2) and s-CAV(2) follows s-CAV(3). Fig. 11(a) demonstrates the results of the example with 1.0 s resolution, which involves three s-CAVs (1–3) that initially drove on three lanes separately. To better present the synchronization process, we plotted the vehicle trajectories of s-CAVs and neighbor vehicles in Fig. 11(b). We observed that s-CAV(3), s-CAV(2) and s-CAV(1) initially drove on lane 1, 2, and 3, respectively. s-CAV(3) and s-CAV(2) drove behind s-CAV(2). Under the synchronization control, s-CAV(3) and s-CAV(2) caught up with s-CAV(1). Then, s-CAV(3) cut in front of s-CAV(2) from lane 1 to lane 2, and eventually, both s-CAV(2) and s-CAV(3) altogether cut in front of s-CAV(1) from lane 2 to lane 3 and form a three-vehicles platoon. The synchronization process took 16 s to complete. From the trajectories of the three s-CAVs, we observed that the switching path of the hybrid MPC system is directly from MPC-I to MPC-III because all s-CAVs switched from the catch-up state to the platooning state

simultaneously. Based on these observations, we confirmed the validity of the new MPC (57) and the hybrid MPC system for multivehicle synchronization.

9. Conclusion

This paper developed a CAV synchronization control, which cooperatively instructs the movements of two CAVs, initially apart and separated by other vehicles in a CAV and HDV mixed traffic flow, so that they can approach each other quickly and then keep a stable car-following mode. Mathematically, the synchronization control is modeled as an MPC system embedded with a mixed-integer nonlinear program (MINLP-MPC), which predicts the surrounding traffic and generates discrete optimal trajectory control laws to have the two s-CAVs catch up and synchronize their movement without jeopardizing the traffic efficiency. To couple the microscopic trajectory control and macroscopic traffic impact involved in the synchronization control, the MPC system introduces binary variables to capture the interactions between microscopic vehicle dynamics, i.e., subject CAVs and their neighbor vehicles, and macroscopic traffic propagation. We proved the recursive feasibility of the MPC model, through which we also demonstrated the applicability of the MPC system in reality. Furthermore, the optimizer of the MPC involves multiple objectives that co-consider several aspects of the traffic and synchronization efficiency. To generate a well-balanced optimal control, this study transfers the initial MPC to a hybrid MPC system, which consists of two sequential MPCs to decorrelate the objective items. Built upon that, we contribute an adaptive weighting strategy for each MPC system which enables us to adaptively tune the control priorities according to the initial traffic condition at each control time step. The proposed MPC, hybrid MPC system, and weighting schemes were further generalized to address multi-vehicle synchronization with a predefined order and target lane.

The experiments based on the field data validate the effectiveness and merits of the synchronization control. Mainly, the synchronization control combined with the adaptive weighting strategy renders more space to trade a little traffic efficiency for a great improvement in the synchronization performance compared with three other strategies (S1-bal, S2-syn and S3-trf) that have fixed weights. The sensitivity analyses on the congestion levels demonstrate that the time needed to complete the synchronization stays relatively stable when traffic is light or mildly congested, i.e., $v/c \ \langle \ 0.55$, but increases significantly when traffic is highly congested, i.e., $v/c \ \rangle 0.75$. We also examined the effect of CAV penetration. The results indicate that more CAV presenting in the traffic can help improve the synchronization efficiency, but this positive effect diminishes. Moreover, we investigated how the communication range affects the performance of synchronization control. The results indicate that 150 m is the rational communication range to trigger the synchronization control, and a longer range only leads to minor improvement but raises the computation load. Last, we conducted a case study on three-vehicle synchronization. Based on the generated vehicle trajectories, we validated the effectiveness of the generalized hybrid MPC system.

This is our first attempt to work on this synchronization control. It motivates several interesting future research topics to develop this study further. For example, one of our future studies seeks to make synchronization control more resilient to communication delay and sensing error. The synchronization control depends on sensing and monitoring the neighboring vehicles' real-time movement. Even though MPC itself, as a discrete closed-loop feedback control system, can handle a certain level of prediction error and uncertainties, there are more advanced approaches to factor in those issues better. Furthermore, the synchronization control relies on a predefined vehicle order in the target platoon. This study can be further extended to adaptively determine the vehicle order and the synchronization control. This extended study will significantly complicate the MPC and solution approaches, and we propose to develop a structured sequential MPC system to address these new challenges in our future studies Fig. 12.

CRediT authorship contribution statement

Jiahua Qiu: Investigation, Writing – original draft, Writing – review & editing. **Lili Du:** Methodology, Supervision, Writing – original draft, Writing – review & editing.

Acknowledgment

This study is partially supported by National Science Foundation, awards CMMI 1818526 (Previous: 1554559) and CMMI 1901994.

Appendix A. Logical Conditions

In this appendix we reformulate logical conditions (5), (6) and (32), (33) by sets of integer constraints. Logical condition (5) models the relationship among binary variable $\rho_{j,j}^l(t)$, relative positions and lane memberships of vehicle j and vehicle j'. It can be reformulated into constraint set (61) by introducing sufficient big value M.

$$x_{j}'(t) - x_{j}(t) \le M\rho_{j,j}^{l}(t) + M\left(1 - \gamma_{j}^{l}(t)\right) + M\left(1 - \gamma_{j}^{l}(t)\right), \ \forall j,j' \in J, l \in L$$
(61.1)

$$x_{j}'(t) - x_{j}(t) \ge M\left(\rho_{j,j}^{l}(t) - 1\right), \ \forall j, j' \in J, l \in L$$
 (61.2)

$$\gamma_{j}^{l}(t) \ge \rho_{i,j}^{l}(t), \ \gamma_{j}^{l}(t) \ge \rho_{i,j}^{l}(t), \ \forall j,j \in J, l \in L$$
 (61.3)

To reformulate the logical condition (6), we introduce another binary variable $\xi_k^l(t) = \rho_{jk}^l(t)\rho_{kj'}^l(t)$, which takes value one when vehicle j' is in the downstream of vehicle j and there exists a vehicle k between them. It can be formulated by the following constraint set (62)

$$\xi_k^l(t) \le \rho_{ik}^l(t) \ \forall j,j' \in J, \ l \in L$$
 (62.1)

$$\xi_{k}^{l}(t) \le \rho_{k'}^{l}(t) \ \forall j, j' \in J, \ l \in L$$
 (62.2)

$$\xi_k^l(t) \ge \rho_{ik}^l(t) + \rho_{ij'}^l(t) - 1 \ \forall j, j' \in J, \ l \in L$$
 (62.3)

Next, we reformulate the logical condition (6) into constraint set (63), where $\delta_{i,i}^l$ is auxiliary binary variable.

$$\delta_{i,l}^l(t) \ge \eta_{i,l}^l(t) \ \forall j,j' \in J, \ l \in L$$

$$\rho_{j,j}^{l}(t) \ge \eta_{j,j}^{l}(t) \ \forall j,j' \in J, \ l \in L$$
(63.2)

$$\eta_{ij'}^l(t) \ge \rho_{ij'}^l(t) + \delta_{ij'}^l(t) - 1 \ \forall j, j' \in J, \ l \in L$$
 (63.3)

$$\sum_{k \in J/\{j,j'\}} \xi_k^l(t) \le \left(1 - \delta_{j,j'}^l(t)\right) M \ \forall j,j' \in J, \ l \in L$$
 (63.4)

$$1 - \sum_{k \in J/\{i,j'\}} \xi_k^l(t) \le \delta_{j,j'}^l(t) \ \forall j,j' \in J, \ l \in L$$
 (63.5)

Finally, logical conditions (32) can be reformulated by the constraint set (64) with a sufficient large number *M*. Condition (33) can also be reformulated as similar to constraint (64.1) as in constraint (64.3).

$$\underline{x}_{c}^{l} + M\left(\phi_{i,c}^{l}(t) - 1\right) \le x_{i}(t) \le \overline{x}_{c}^{l} + M\left(1 - \phi_{i,c}^{l}(t)\right), \ \forall i \in I, l \in L, c \in C_{l}$$
(64.1)

$$\underline{y}_{c}^{l} + M(\phi_{i,c}^{l}(t) - 1) \le y_{i}(t) \le \overline{y}_{c}^{l} + M(1 - \phi_{i,c}^{l}(t)), \ \forall i \in I, l \in L, c \in C_{l}$$
(64.2)

$$\underline{x}_{c}^{l} + M\left(\phi_{\omega,c}^{l}(t) - 1\right) \leq \widehat{x}_{\omega}(t) \leq \overline{x}_{c}^{l} + M\left(1 - \phi_{\omega,c}^{l}(t)\right), \ \forall i \in I, l \in L, c \in C_{l}$$

$$(64.3)$$

Appendix B. Minimum spacing of scenario I

In this Appendix, we derive the spacing $s_{\omega,1}(t+nk)$ according to the Equation set (52). The results are presented in Table 6, where $\Delta s_{\omega,i}(t)$ is the spacing difference of current spacing to the previous spacing, i.e., $\Delta s_{\omega,i}(t+nk) = s_{\omega,i}(t+nk) - s_{\omega,i}(t+(n-1)k)$. The results indicate that the minimum spacing is at n=5.

Appendix C. Calculation of v/c by Greenshield Model

In this Appendix, we introduce how to calculate the v/c based on the traffic information of testing cases. Recall that we randomly select road segments in the NGSIM dataset to generate testing cases. Each testing case contains the information of flow density, vehicle spacings and vehicle velocities. Based on this information, we estimate the congestion level (i.e., the traffic volume (v) to capacity (c) ratio) of each testing case through Greenshield model in Eq. (65), where k_i is the jam density and k is the density.

$$\frac{v}{c} = \frac{4c}{k_j} k - \frac{4c}{k_i^2} k^2 \tag{65}$$

The jam density k_i and capacity c adopt the values in Table 2.

Appendix D. Performance of Synchronization Control under Different CACC Schemes

In Section 4.3, we adopt a first-order model derived by PATH to model the CACC car-following behavior (Milanés and Shladover, 2014) since this control scheme is derived by fitting the data obtained from the field experiments and it is confirmed to have good performance in capturing the car-following movement of current commercially available CACC systems. To examine the performance of synchronization control when n-CAVs follow a different CACC scheme, we conduct the experiment by using another CACC scheme (Chen et al., 2019). In this CACC scheme, The moving dynamics of n-CAV(ω) are modeled as follows.

$$a_{\omega}(t) = K_{v}(\widehat{v}_{j}(t) - \overline{v_{x}}) + K_{s}(\widehat{x}_{j}(t) - \widehat{x}_{\omega}(t) - s_{d}) \ \forall \omega \in \Omega_{c}^{l}$$

$$(66)$$

where j is the preceding vehicle of neighboring vehicle ω ; K_{ν} and K_{s} are the positive gains of the speed term and the spacing term; s_{d} is the desired gap.

In this experiment, we set $K_{\nu} = 0.58s^{-1}$, $K_{\rm S} = 0.1s^{-1}$ and $s_d = 20m$ according to (Chen et al., 2019). The figures below compare the synchronization time and average traffic speed using this new CACC scheme (CACC-2) with those using the CACC scheme (CACC-1) adopted in the Section 4.3. We can observe that the synchronization controller still works and follows a similar trend under two scenarios. It indicates that different CACC schemes won't affect the trend of the results since most CACC schemes provide similar expected benefits to the synchronization process as discussed at the end of Section 4.3.

References

Abdolmaleki, M., Masoud, N., Yin, Y., 2019. Vehicle-to-vehicle wireless power transfer: paving the way toward an electrified transportation system. Transp. Res. Part C Emerg. Technol. 103, 261–280.

Alsuhaim, A., Rayamajhi, A., Westall, J., Martin, J., 2021. Adapting time headway in cooperative adaptive cruise control to network reliability. IEEE Trans. Veh. Technol. 70, 12691–12702.

Ashtiani, F., Fayazi, S.A., Vahidi, A., 2018. Multi-intersection traffic management for autonomous vehicles via distributed mixed integer linear programming. In: Proceedings of the Annual American Control Conference (ACC), pp. 6341–6346.

Awal, T., Murshed, M., Ali, M., 2015. An efficient cooperative lane-changing algorithm for sensor-and communication-enabled automated vehicles. In: Proceedings of the IEEE Intelligent Vehicles Symposium (Iv), pp. 1328–1333.

Badnava, S., Meskin, N., Gastli, A., Al-Hitmi, M., Ghommam, J., Mesbah, M., Mnif, F., 2021. Platoon Transitional Maneuver Control System: A Review. IEEE Access. Balal, E., Cheu, R.L., Sarkodie-Gyan, T., 2016. A binary decision model for discretionary lane changing move based on fuzzy inference system. Transp. Res. Part C Emerg. Technol. 67, 47–61.

Bang, S., Ahn, S., 2017. Platooning strategy for connected and autonomous vehicles: transition from light traffic. Transp. Res. Rec. 2623, 73–81.

Bevly, D., Cao, X., Gordon, M., Ozbilgin, G., Kari, D., Nelson, B., Woodruff, J., Barth, M., Murray, C., Kurt, A., 2016. Lane change and merge maneuvers for connected and automated vehicles: a survey. IEEE Trans. Intell. Veh. 1, 105–120.

Bhoopalam, A.K., Agatz, N., Zuidwijk, R., 2018. Planning of truck platoons: a literature review and directions for future research. Transp. Res. B Methodol. 107, 212–228.

Cao, W., Mukai, M., Kawabe, T., Nishira, H., Fujiki, N., 2015. Cooperative vehicle path generation during merging using model predictive control with real-time optimization. Control Eng. Pract. 34, 98–105.

Chen, J., Zhao, P., Mei, T., Liang, H., 2013. Lane change path planning based on piecewise bezier curve for autonomous vehicle. In: Proceedings of the IEEE International Conference on Vehicular Electronics and Safety, ICVES 2013. https://doi.org/10.1109/ICVES.2013.6619595.

Chen, J., Zhou, Y., Liang, H., 2019. Effects of ACC and CACC vehicles on traffic flow based on an improved variable time headway spacing strategy. IET Intel. Transport. Syst. 13, 1365–1373.

Choi, S., Yeo, H., 2017. Framework for simulation-based lane change control for autonomous vehicles. In: Proceedings of the IEEE Intelligent Vehicles Symposium (IV), pp. 699–704.

Čičić, M., Johansson, K.H., 2019. Energy-optimal platoon catch-up in moving bottleneck framework. In: Proceedings of the 18th European Control Conference (ECC), pp. 3674–3679.

Daganzo, C.F., 1995. The cell transmission model, part II: network traffic. Transp. Res. B Methodol. 29, 79–93.

Dey, K.C., Yan, L., Wang, X., Wang, Y., Shen, H., Chowdhury, M., Yu, L., Qiu, C., Soundararaj, V., 2015. A review of communication, driver characteristics, and controls aspects of cooperative adaptive cruise control (CACC). IEEE Trans. Intell. Transp. Syst. 17, 491–509.

Firozzi, R., Zhang, X., Borrelli, F., 2021. Formation and reconfiguration of tight multi-lane platoons. Control Eng. Pract. 108, 104714.

Ganaoui-Mourlan, E., Camp, S., Hannagan, T., Arora, V., de Neuville, M., Kousournas, V.A., 2021. Path planning for autonomous platoon formation. Sustainability 13, 4668.

Goli, M., Eskandarian, A., 2020. Merging strategies, trajectory planning and controls for platoon of connected, and autonomous vehicles. Int. J. Intell. Transp. Syst. Res. 18, 153–173.

Gong, S., Du, L., 2018. Cooperative platoon control for a mixed traffic flow including human drive vehicles and connected and autonomous vehicles. Transp. Res. B Methodol. 116, 25–61.

Gong, S., Du, L., 2016. Optimal location of advance warning for mandatory lane change near a two-lane highway off-ramp. Transp. Res. B Methodol. 84, 1–30. Gong, S., Shen, J., Du, L., 2016. Constrained optimization and distributed computation based car following control of a connected and autonomous vehicle platoon. Transp. Res. B Methodol. 94, 314–334.

Graffione, S., Bersani, C., Sacile, R., Zero, E., 2020. Model Predictive Control for Cooperative Insertion or Exit of a Vehicle in a Platoon. ICINCO, pp. 352–359. Hidalgo, C., Lattarulo, R., Flores, C., Pérez Rastelli, J., 2021. Platoon merging approach based on hybrid trajectory planning and CACC strategies. Sensors 21, 2626.

Findingo, C., Lattartio, R., Fores, C., Perez Rastein, J., 2021. Platoon merging approach based on hybrid trajectory planning and CACC strategies. Sensors 21, 262. Ho, K.Y., Kang, P.C., Hsu, C.H., Lin, C.H., 2010. Implementation of WAVE/DSRC devices for vehicular communications. In: Proceedings of the International Symposium on Computer, Communication, Control and Automation (3CA), pp. 522–525.

Hallmark, S., Veneziano, D., Litteral, T., 2019. Preparing local agencies for the future of connected and autonomous vehicles (No. MN/RC 2019-18). Dept. of Transportation. Research Services & Library, Minnesota.

Horowitz, R., Tan, C.W., Sun, X., 2004. An Efficient Lane Change Maneuver for Platoons of Vehicles in An Automated Highway System, IMECE2003-41845, pp. 355–362.

Hu, G., Wang, F., Lu, W., Kwembe, T.A., Whalin, R.W., 2020. Cooperative bypassing algorithm for connected and autonomous vehicles in mixed traffic. IET Intel. Transport Syst. 14, 915–923.

Kianfar, R., Falcone, P., Fredriksson, J., 2015. A control matching model predictive control approach to string stable vehicle platooning. Control Eng. Pract. 45, 163–173.

Knights, V.A., Gacovski, Z., Deskovski, S., Petrovska, O., 2018. Guidance and control system for platoon of autonomous mobile robots. J. Electr. Eng. 6, 281–288. Li, L., Gan, J., Qu, X., Mao, P., Yi, Z., Ran, B., 2021. A novel graph and safety potential field theory-based vehicle platoon formation and optimization method. Appl. Sci. 11, 958.

Li, Q., Chen, Z., Li, X., 2022a. A review of connected and automated vehicle platoon merging and splitting operations. IEEE Trans. Intell. Transp. Syst. 23 (11), 22790–22806.

Li, Q., Li, X., 2022. Trajectory planning for autonomous modular vehicle docking and autonomous vehicle platooning operations. Transp. Res. E Logist. Transp. Rev. 166, 102886.

Li, Q., Li, X., Huang, Z., Halkias, J., McHale, G., James, R., 2022b. Simulation of mixed traffic with cooperative lane changes. Comput. Aided Civ. Infrastruct. Eng. 37, 1978–1996.

- Li, T., Wu, J., Chan, C.-Y., Liu, M., Zhu, C., Lu, W., Hu, K., 2020a. A cooperative lane change model for connected and automated vehicles. IEEE Access 8, 54940–54951.
- Li, Y., Chen, W., Peeta, S., Wang, Y., 2019. Platoon control of connected multi-vehicle systems under V2X communications: design and experiments. IEEE Trans. Intell. Transp. Syst. 21, 1891–1902.
- Li, Y., Zhong, Z., Song, Y., Sun, Q., Sun, H., Hu, S., Wang, Y., 2020b. Longitudinal platoon control of connected vehicles: analysis and verification. IEEE Trans. Intell. Transp. Syst. 23, 4225–4235.
- Liang, K.Y., Mårtensson, J., Johansson, K.H., 2015. Heavy-duty vehicle platoon formation for fuel efficiency. IEEE Trans. Intell. Transp. Syst. 17, 1051–1061.
- Liu, P., Kurt, A., Ozguner, U., 2018. Synthesis of a behavior-guided controller for lead vehicles in automated vehicle convoys. Mechatronics 50, 366-376.
- Liu, P., Özgüner, Ü., 2015. Predictive control of a vehicle convoy considering lane change behavior of the preceding vehicle. In: Proceedings of the American Control Conference (ACC), pp. 4374–4379.
- Lu, H., Song, G., Yu, L., 2018. The "acceleration cliff": an investigation of the possible error source of the VSP distributions generated by Wiedemann car-following model. Transp. Res. D Transp. Environ. 65, 161–177.
- Maglogiannis, V., Naudts, D., Hadiwardoyo, S., van den Akker, D., Marquez-Barja, J., Moerman, I., 2021. Experimental V2X evaluation for C-V2X and ITS-G5 technologies in a real-life highway environment. IEEE Trans. Netw. Serv. Manag. 19, 1521–1538.
- Maiti, S., Winter, S., Kulik, L., Sarkar, S., 2019. The impact of flexible platoon formation operations. IEEE Trans. Intell. Veh. 5, 229-239.
- Manual, H.C., 2000. Highway capacity manual. Washington, DC 2 (1).
- Marcucci, T., Tedrake, R., 2020. Warm start of mixed-integer programs for model predictive control of hybrid systems. IEEE Trans. Automat. Contr. 66, 2433–2448. Maxim, A., Caruntu, C.F., Lazar, C., 2017. Cruise and headway control for vehicle platooning using a distributed model predictive control algorithm. In: Proceedings of the 21st International Conference on System Theory, Control and Computing (ICSTCC). pp, pp. 146–151.
- Mayne, D.Q., 2014. Model predictive control: recent developments and future promise. Automatica 50, 2967-2986.
- Meng, D., Song, G., Wu, Y., Zhai, Z., Yu, L., Zhang, J., 2021. Modification of Newell's car-following model incorporating multidimensional stochastic parameters for emission estimation. Transp Res D Transp Environ 91, 102692.
- Milanés, V., Godoy, J., Villagrá, J., Pérez, J., 2010. Automated on-ramp merging system for congested traffic situations. IEEE Trans. Intell. Transp. Syst. 12, 500–508. Milanés, V., Shladover, S.E., 2014. Modeling cooperative and autonomous adaptive cruise control dynamic responses using experimental data. Transp Res Part C Emerg Technol 48, 285–300.
- Mu, C., Du, L., Zhao, X., 2021. Event triggered rolling horizon based systematical trajectory planning for merging platoons at mainline-ramp intersection. Transp Res Part C Emerg Technol 125. https://doi.org/10.1016/j.trc.2021.103006.
- Naus, G.J.L., Vugts, R.P.A., Ploeg, J., van de Molengraft, M.J.G., Steinbuch, M., 2010. String-stable CACC design and experimental validation: a frequency-domain approach. IEEE Trans. Veh. Technol. 59, 4268-4279.
- Negenborn, R.R., Maestre, J.M., 2014. Distributed model predictive control: an overview and roadmap of future research opportunities. IEEE Control Syst. Mag. 34, 87–97.
- Ni, J., Han, J., Dong, F., 2020. Multivehicle cooperative lane change control strategy for intelligent connected vehicle. J Adv Transp 2020, 1–10.
- Nie, J., Zhang, J., Ding, W., Wan, X., Chen, X., Ran, B., 2016. Decentralized cooperative lane-changing decision-making for connected autonomous vehicles. IEEE access 4, 9413–9420.
- Nilsson, J., Brännström, M., Fredriksson, J., Coelingh, E., 2016. Longitudinal and lateral control for automated yielding maneuvers. IEEE Trans. Intell. Transp. Syst. 17. 1404–1414.
- Nilsson, J., Falcone, P., Ali, M., Sjöberg, J., 2015. Receding horizon maneuver generation for automated highway driving. Control Eng. Pract. 41, 124-133.
- Pasquale, C., Sacone, S., Siri, S., Ferrara, A., 2018. A new Micro-Macro METANET model for platoon control in freeway traffic networks. In: Proceedings of the 21st International Conference on Intelligent Transportation Systems (ITSC), pp. 1481–1486.
- Peters, A.A., Middleton, R.H., Mason, O., 2014. Leader tracking in homogeneous vehicle platoons with broadcast delays. Automatica 50, 64-74.
- Piacentini, G., Ferrara, A., Papamichail, I., Papageorgiou, M., 2019a. Highway traffic control with moving bottlenecks of connected and automated vehicles for travel time reduction. In: Proceedings of the IEEE 58th Conference on Decision and Control (CDC), pp. 3140–3145.
- Piacentini, G., Goatin, P., Ferrara, A., 2018. Traffic control via moving bottleneck of coordinated vehicles. IFAC PapersOnLine 51, 13-18.
- Piacentini, G., Pasquale, C., Sacone, S., Siri, S., Ferrara, A., 2019b. Multiple moving bottlenecks for traffic control in freeway systems. In: Proceedings of the 18th European Control Conference (ECC), pp. 3662–3667.
- Police Radar Information Center, 2020. Acceleration Parameters [WWW Document]. Police Radar Information Center. URL. https://copradar.com/chapts/references/acceleration.html.
- Qin, Y., Wang, H., Ni, D., 2021. Lighthill-Whitham-Richards model for traffic flow mixed with cooperative adaptive cruise control vehicles. Transp. Sci. 55, 883–907. Raboy, K., Ma, J., Leslie, E., Zhou, F., 2021. A proof-of-concept field experiment on cooperative lane change maneuvers using a prototype connected automated vehicle testing platform. J. Intell. Transp. Syst. 25, 77–92.
- Rahman, M., Chowdhury, M., Dey, K., Islam, M.R., Khan, T., 2017. Evaluation of driver car-following behavior models for cooperative adaptive cruise control systems. Transp. Res. Rec. 2622, 84–95.
- Rawlings, J.B., Mayne, D.Q., Diehl, M., 2017. Model Predictive Control: Theory, Computation, and Design. Nob Hill Publishing Madison, WI.
- Rios-Torres, J., Malikopoulos, A.A., 2016. A survey on the coordination of connected and automated vehicles at intersections and merging at highway on-ramps. IEEE Trans. Intell. Transp. Syst. 18, 1066–1077.
- Shao, Y., Sun, Z., 2020. Eco-approach with traffic prediction and experimental validation for connected and autonomous vehicles. IEEE Trans. Intell. Transp. Syst. 22, 1562–1572.
- Sharath, M.N., Velaga, N.R., 2020. Enhanced intelligent driver model for two-dimensional motion planning in mixed traffic. Transp Res Part C Emerg Technol 120, 102780.
- Subedi, B., Gaweesh, S.M., Yang, G., Ahmed, M.M., 2020. Connected vehicle training framework and lessons learned to improve safety of highway patrol troopers. Transp. Res. Res. 2674, 447–463.
- Sun, W., Wang, S., Shao, Y., Sun, Z., Levin, M.W., 2022. Energy and mobility impacts of connected autonomous vehicles with co-optimization of speed and powertrain on mixed vehicle platoons. Transp Res Part C Emerg Technol 142, 103764.
- Talebpour, A., Mahmassani, H.S., Hamdar, S.H., 2015. Modeling lane-changing behavior in a connected environment: a game theory approach. Transp. Res. Procedia 7, 420–440.
- Tomas-Gabarron, J.B., Egea-Lopez, E., Garcia-Haro, J., 2013. Vehicular trajectory optimization for cooperative collision avoidance at high speeds. IEEE Trans. Intell. Transp. Syst. 14, 1930–1941.
- Tuchner, A., Haddad, J., 2017. Vehicle platoon formation using interpolating control: a laboratory experimental analysis. Transp Res Part C Emerg Technol 84, 21–47. Vahidi, A., Sciarretta, A., 2018. Energy saving potentials of connected and automated vehicles. Transp Res Part C Emerg Technol 95, 822–843.
- Wang, C., Dai, Y., Xia, J., 2020. A CAV platoon control method for isolated intersections: guaranteed feasible multi-objective approach with priority. Energies 13. https://doi.org/10.3390/en13030625. Basel.
- Wang, M., Daamen, W., Hoogendoorn, S.P., van Arem, B., 2014. Rolling horizon control framework for driver assistance systems. Part I: mathematical formulation and non-cooperative systems. Transp Res Part C Emerg Technol 40. https://doi.org/10.1016/j.trc.2013.11.023.
- Wang, M., Hoogendoorn, S.P., Daamen, W., van Arem, B., Happee, R., 2015. Game theoretic approach for predictive lane-changing and car-following control. Transp Res Part C Emerg Technol 58, 73–92.
- Wang, Y., Liu, Z., Zuo, Z., Li, Z., Wang, L., Luo, X., 2019. Trajectory planning and safety assessment of autonomous vehicles based on motion prediction and model predictive control. IEEE Trans. Veh. Technol. 68, 8546–8556.
- Wang, Z., Wu, G., Barth, M.J., 2018. A review on cooperative adaptive cruise control (CACC) systems: architectures, controls, and applications. In: Proceedings of 21st International Conference on Intelligent Transportation Systems (ITSC), pp. 2884–2891.

- Wei, Y., Avc\i, C., Liu, J., Belezamo, B., Ayd\in, N., Li, P.T., Zhou, X., 2017. Dynamic programming-based multi-vehicle longitudinal trajectory optimization with simplified car following models. Transp. Res. Part B Methodol. 106, 102–129.
- Woo, S., Skabardonis, A., 2021. Flow-aware platoon formation of connected automated vehicles in a mixed traffic with human-driven vehicles. Transp. Res. Part C Emerg. Technol. 133, 103442.
- Wu, C., Xu, Z., Liu, Y., Fu, C., Li, K., Hu, M., 2020. Spacing policies for adaptive cruise control: a survey. IEEE Access 8. https://doi.org/10.1109/ ACCESS 2020 2978244
- Xiao, L., Gao, F., 2011. Practical string stability of platoon of adaptive cruise control vehicles. IEEE Trans. Intell. Transp. Syst. 12, 1184–1194.
 Xiao, L., Wang, M., van Arem, B., 2017. Realistic car-following models for microscopic simulation of adaptive and cooperative adaptive cruise control vehicles. Transp. Res. Rec. 2623, 1-9.
- Yan, M., Song, J., Zuo, L., Yang, P., 2017. Neural adaptive sliding-mode control of a vehicle platoon using output feedback. Energies 10, 1906. Basel.
- Yang, H., Rakha, H., Ala, M.V., 2016. Eco-cooperative adaptive cruise control at signalized intersections considering queue effects. IEEE Trans. Intell. Transp. Syst. 18, 1575-1585.
- Zhang, H., Du, L., Shen, J., 2022. Hybrid MPC system for platoon based cooperative lane change control using machine learning aided distributed optimization. Transp. Res. B 159, 104-142.
- Zhuang, W., Xu, L., Yin, G., 2020. Robust cooperative control of multiple autonomous vehicles for platoon formation considering parameter uncertainties. Automot. Innov. 3, 88-100.
- Zimmermann, M., Schopf, D., Lütteken, N., Liu, Z., Storost, K., Baumann, M., Happee, R., Bengler, K.J., 2018. Carrot and stick: a game-theoretic approach to motivate cooperative driving through social interaction. Transp. Res. Part C Emerg. Technol. 88, 159-175.
- Zohdy, I.H., Rakha, H., 2012. Game theory algorithm for intersection-based cooperative adaptive cruise control (CACC) systems. In: Proceedings of 15th International ${\tt IEEE}\ Conference\ on\ Intelligent\ Transportation\ Systems,\ pp.\ 1097-1102.$